J. Fluid Mech. (1992), *vol.* 239, *pp.* 551–606
Printed in Great Britain

Acoustic streaming in the ear itself

By JAMES LIGHTHILL
Department of Mathematics, University College, Gower Street, London WC1E 6BT, UK

(Received 17 June 1991)

Just as mean motions, usually described as acoustic streaming, can be generated by sound waves, so also those cochlear travelling waves into which incident sound waves are converted in the liquid-filled mammalian inner ear are capable of generating mean motions. These predominate, for acoustic components of each frequency ω, near the characteristic place where the wave energy E per unit length rises rather steeply to a maximum $E^{\max}$ before dropping precipitously to zero.

Even though the nature of cochlear travelling waves, as determined (above all) by the sharply and continuously falling distribution of stiffness for the basilar membrane vibrating within the cochlear fluids, is very different from that of ordinary sound waves (see §§2, 3 and 4 respectively for energy distribution along the length of the cochlea, over a cochlear cross-section and within boundary layers), nevertheless a comprehensive analysis of mean streaming motions in the cochlea shows them to be governed by remarkably similar laws. The expression

$$\tfrac{1}{4}V^2 c^{-1} - \tfrac{3}{4}V(\mathrm{d}V/\mathrm{d}x)\,\omega^{-1}$$

(equation (1)) appropriate to a wave travelling in the x-direction with velocity amplitude $V(x)$, as obtained by Rayleigh (1896) for the mean acoustic-streaming velocity just outside a boundary layer due to wave dissipation therein, remains a good approximation (see §§5 and 6 – with some modest corrections, at low or at high wavenumbers respectively, analysed in §§7 and 8) for travelling waves in the cochlea; where, however, the decrease of their phase velocity c to low values near the characteristic place conspires with the increase of V to enhance streaming there.

Farther from the boundary layer attached to the basilar membrane, the mean streaming is derived (§9) as a low-Reynolds-number motion compatible with the distribution (1) of 'effective slip velocity' at the boundary. This velocity's precipitous fall to zero at the characteristic place is shown (§§9 and 10) to produce there a mean volume outflow

$$q = \frac{0.15E^{\max}}{\rho(\omega\nu)^{\frac{1}{2}}L}$$

(equation (160)) per unit length of the basilar membrane into the scala media; here, ρ and ν are the endolymph's density and kinematic viscosity (essentially, those of water) and L is the e-folding distance for basilar-membrane stiffness.

Equation (160), derived here for a freely propagating wave (and so not allowing for enhancements from any travelling-wave amplification – discussed qualitatively in §3 – due to forcing by vibrations of outer hair cells) is the main conclusion of this paper. Physiological questions of whether this flow q may be channelled through the space between the tectorial membrane and inner hair cells, whose stereocilia may therefore be stimulated by a mean deflecting force, are noted here but postponed for detailed consideration in a later paper.

CONTENTS

1. Introduction

Mean motions of fluid induced by sound waves are called acoustic streaming (see Lighthill 1978*a* for a detailed survey, and Lighthill 1978*b*, §4.7 for a synopsis, in the wider context of waves in fluids, of steady streaming generated by wave attenuation). But, in healthy mammalian ears, sound waves incident on the eardrum are converted by the middle ear's linkage mechanism into cochlear travelling waves, that propagate vibratory movements of the basilar membrane within the inner-ear fluids (see Lighthill 1991 and references therein). This is a paper concerned with estimating the magnitude of any mean streaming motions generated by acoustic signals after conversion into cochlear travelling waves.

The purposes of such estimation are mainly biological, being indicated in §2 below. Briefly, the study is motivated by observations (K. Å. I. Flock 1988, personal communication) showing that the transduction function of inner hair cells – that is, their ability to stimulate neural activity on reception of a signal – can be brought into sustained operation even by steady deflection of their stereocilia. It is a challenge, therefore, to investigate whether attenuation of the cochlear travelling wave can generate mean streaming motions, and to estimate their magnitudes, with the purpose of investigating whether they can play a role in inner-hair-cell transduction by such deflection of stereocilia.

The present paper, however, concentrates upon the use of theoretical fluid mechanics to estimate the mean streaming motions (their detailed biological implications being left for consideration elsewhere). It is above all the highly specialized nature of the living mammalian cochlea, and the strictly limited capability of presently available techniques for making *in vivo* observations of its fluid motions, that constrain us to employ theoretical methods.

Fortunately, the analysis proves to be both tractable and also of sufficiently wide interest to be appropriate for presentation to a general fluid-mechanics readership. As the title of this paper implies, it turns out that, notwithstanding the conversion of acoustic signals in air into waves of a quite different type (with fluid motions more

like those in water waves) in the aqueous medium of the cochlea, nevertheless the fundamentals of acoustic-streaming theory remain rather closely applicable in this different system. Streaming gains very substantially in importance, however, because of the greatly reduced wave speed.

Indeed for each pure-tone component of an acoustic signal, say with frequency ω, the velocity of the cochlear travelling wave tends towards zero at a particular place: the characteristic place for that frequency. Furthermore, the wave amplitude increases as this place is approached, and both these features are found to increase the local magnitude of mean streaming motions. It follows that analysis needs to concentrate particularly on the streaming generated by acoustic components of each frequency near the characteristic place for that frequency – which, too, is where they may (possibly) be important for inner-hair-cell transduction.

This is a region where, on either side of the basilar membrane, fluid motions are considered (see the review by Lighthill 1991, for example) to be rather similar (on greatly different scales, of course) to those associated with the propagation of surface waves on deep water; although with the wavy motions of the free surface replaced by those of the basilar membrane and with the role of (say) gravity as restoring force replaced by the corresponding stiffness properties of the basilar membrane, whose inertia, also, needs to be taken into account. It is the stiffness decrease along the length of the cochlea – a decrease by close on four orders of magnitude between base (where the wave originates) and apex – that initiates the reduction in wave speed.

Near the characteristic place, moreover, the effective impedance of the basilar membrane is diminished to a value even less than the local stiffness by an inertial component, allowing an even bigger reduction in the waves' phase velocity c. Also, the velocity U of energy propagation (group velocity) is reduced still more, allowing wave energy density – and therefore amplitude – to increase dramatically, before they ultimately decay to zero as the result of a powerful action of viscous dissipation on the greatly slowed-down wave.

Now, where wave energy is sharply attenuated, theoretical fluid mechanics suggests a general likelihood of the appearance of streaming motions. Indeed, the knowledge that waves in fluids necessarily transport momentum – the momentum flow rate being obtained by dividing energy flow by phase velocity – may give an expectation that, where wave energy is dissipated, the corresponding wave momentum becomes converted into a mean motion. For example, steep attenuation in a powerful ultrasonic beam is known (Lighthill 1978*a*) to convert its momentum flow into a jet-like form of acoustic streaming.

By contrast, viscous attenuation at rather lower frequencies is insignificant in the body of the fluid, being effectively confined to thin Stokes boundary layers. A somewhat different form of acoustic streaming then results (Lighthill 1978*b*, pp. 346–349) from the fact that the forces generating it are concentrated within the interiors of those thin layers attached to solid boundaries. Nevertheless these forces (assuming the form of gradients of Reynolds stresses) produce just outside such a layer a substantial streaming velocity which can be written as

$$\tfrac{1}{4}V^2 c^{-1} - \tfrac{3}{4}V(\mathrm{d}V/\mathrm{d}x)\omega^{-1} \tag{1}$$

if the sound waves' velocity amplitude is taken as $(V(x), 0, 0)$ just outside the layer, where the local distribution (1) of forced streaming motions (sometimes described as 'an effective slip velocity') may act, furthermore, to set up a field of low-Reynolds-number mean motion in its neighbourhood.

A third possible source of streaming is suggested by the above-mentioned analogy

with surface waves on deep water. These are waves where, even when the water's mean motion at any fixed point (the Eulerian mean motion) is zero, the individual particles of fluid have a non-zero mean motion

$$\boldsymbol{u}_{\mathrm{M}} \tag{2}$$

known as the Stokes drift. In more general cases, when these waves are combined with a non-zero Eulerian mean motion $\boldsymbol{u}_{\mathrm{E}}$, the Stokes drift $\boldsymbol{u}_{\mathrm{M}}$ represents the difference

$$\boldsymbol{u}_{\mathrm{M}} = \boldsymbol{u}_{\mathrm{L}} - \boldsymbol{u}_{\mathrm{E}} \tag{3}$$

between the Lagrangian mean motion $\boldsymbol{u}_{\mathrm{L}}$ (the mean velocity for a particle of fluid) and the Eulerian mean motion (mean fluid velocity at a fixed point).

The Stokes drift $\boldsymbol{u}_{\mathrm{M}}$ for deep-water waves takes a familiar exponential form which reaches a maximum V^2c^{-1} (where V is velocity amplitude and c is phase velocity) at the free surface. If expression (3) took such a form for the closely analogous cochlear travelling waves, then it might be imagined that $\boldsymbol{u}_{\mathrm{M}}$ would play a significant role in cochlear streaming. Once the free surface is replaced, however, by a vibrating basilar membrane with boundary layer attached, the total Stokes drift flow outside this boundary layers turns out (§5) to be exactly counterbalanced by an equal and opposite flow inside it.

Accordingly, it turns out that the second of the above three types of acoustic streaming is the one important in the cochlea. A careful study by the Stokes boundary-layer approximation shows it, remarkably enough, to be given by exactly the same expression (1), with V now as the velocity amplitude of the basilar membrane's vibration, wherever the fluid motions are locally two-dimensional; while that expression's generalization to fully three-dimensional motions also takes the same form as it does for acoustic streaming.

The challenge of uncovering the underlying physics of why such different types of streaming take essentially the same form when the boundary-layer approximation is used is faced in §6 below. The physical arguments need care and may be felt to call for verification by rigorous mathematical deduction. Although formal matched-asymptotics procedures could have provided this, a preferable method is to calculate uniformly valid viscous-flow solutions (see the Appendices) which do not depend on the boundary-layer approximation. They have the great advantage of both (i) proving the correctness of equation (1) in that limit where a truly separate Stokes boundary layer is present (its thickness being small compared with the scale of the travelling-wave motions) and (ii) computing those modifications to it which occur at high wavenumbers where no such separation into a boundary layer and an external irrotational flow can exist.

The streaming analysis is preceded by a brief general account (§2) of cochlear biomechanics (see Lighthill 1991 for a much fuller review). This needs to stress first of all that the basilar membrane is by no means 'a membrane' in the mechanics sense; instead, its stiffness properties are highly anisotropic (Voldřich 1978, 1983) in a way that allows neighbouring short sections of the basilar membrane to vibrate almost independently of one another. For each frequency ω this facilitates the above-mentioned continuous decrease, as the characteristic place is approached, in the phase velocity c and therefore also in the local wavelength $\lambda = 2\pi c/\omega$.

Results in this paper, however, are expressed not in terms of such a local wavelength but in terms of the wavenumber

$$k = \omega/c, \tag{4}$$

with its precise definition as the rate of increase in phase lag of basilar-membrane oscillations with distance from the base (origin of the travelling wave); evidently, the wavelength $\lambda = 2\pi/k$ has a less clear-cut meaning for waves with spatially varying properties. At each position, as the wavenumber k becomes large, the frequency ω approaches a constant asymptote (§2) in a way that permits those extremely low values, already mentioned, of the group velocity

$$U = \partial\omega/\partial k. \tag{5}$$

The remarkable recent discovery that, at low sound levels, a physiologically active process (thought to reside in the outer hair cells) amplifies the vibrations of the basilar membrane, is also touched on briefly in §2 (with references). By increasing travelling-wave amplitudes, it is seen as enhancing the potential importance of streaming motions.

Analysis of the travelling wave is based on high-frequency asymptotics (sometimes referred to as the Liouville–Green approximation, or else 'WKB'), and reasons for its expected good accuracy near the characteristic place are given in §2. The three-dimensional distribution of wave energy outside the Stokes boundary layer, based on solutions of the Laplace equation

$$\partial^2\phi/\partial y^2 + \partial^2\phi/\partial z^2 - k^2\phi = 0 \tag{6}$$

for waves of wavenumber k (with y and z as Cartesian coordinates in a cochlear cross-section), is analysed in §3.

At a particular point on the basilar membrane rather close to the characteristic place, these solutions have locally an approximately two-dimensional form, whose continued compatibility with the assumptions of high-frequency asymptotics is verified in §4. Then its modified character within the Stokes boundary layer is explained (with references to Appendix A for uniformly valid viscous-flow solutions at high wavenumbers). Studies in §5 establish the nature of the 'Stokes drift' (3), and show its net mass flow to be zero (a property proved in Appendix B to be exact for all wavenumbers).

The paper's main conclusions for locally two-dimensional flow then follow (as described earlier) in §6, with references to the Appendices for full mathematical proofs. They are extended to general three-dimensional motions in §7. High-wavenumber modifications, such as are computed in detail in Appendix A for energy dissipation rate and in Appendices B and C (respectively) for the two parts of (1), are briefly summarized, with discussion, in §8.

Finally, §9 gives preliminary consideration to the overall low-Reynolds-number mean-flow patterns that may be forced by the streaming motions generated near the solid boundary, and §10 goes on to offer estimates of their magnitudes in the immediate neighbourhoods of inner-hair-cell stereocilia; on the other hand, in this essentially fluid-mechanical paper, all attempts to draw any specific biological conclusions are for the time being deferred for further consideration in possible future joint work with cochlear physiologists.

2. Biomechanics of cochlear travelling waves

Cochlear travelling waves, and their role in the ear's frequency discrimination, were discovered in experiments on cadavers (Békésy 1960) and related to the steeply graded stiffness properties of the basilar membrane vibrating within the cochlear fluids. Later, however, the introduction of specialized techniques allowing measure-

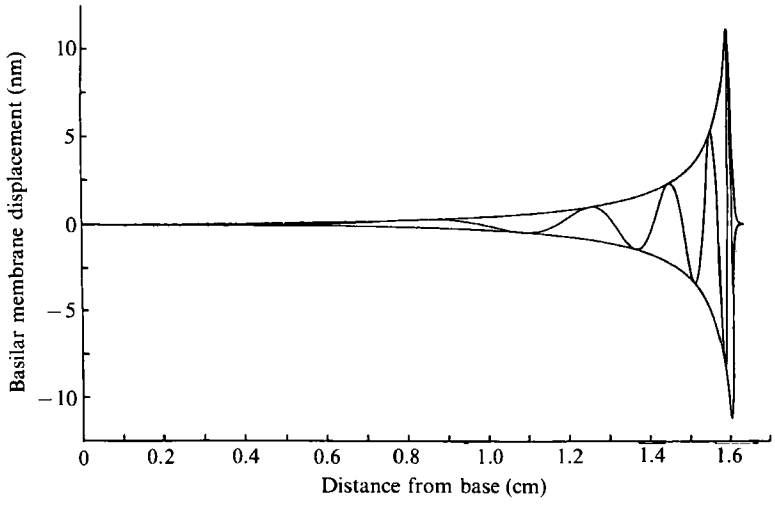

FIGURE 1. Reconstruction by Zweig (1976) of the travelling waves on a squirrel monkey's basilar membrane excited by a pure tone of 70 dB amplitude at a frequency of 2 kHz. The displacement curve for the travelling wave is shown at one instant of time (note the transition from very long to very short waves); the envelope of the travelling wave is also given. This reconstruction is computed from measurements of amplitude and phase made by Rhode (1971), with the use of a reasonable 'smoothing' assumption to interpolate between Rhode's phase measurements at different points of the membrane. Note that the vertical scale is enormously enlarged, being given in nanometres as against a horizontal scale of centimetres.

ments *in vivo* of cochlear response to sound (Johnstone, Taylor & Boyle 1970; Rhode 1971) showed the biomechanics of a living mammalian cochlea to be notably different from the mechanics of a cochlea immediately after death: in response to a pure tone, for example, the build-up in wave amplitude at the characteristic place reached a much sharper peak (higher by 20 to 30 dB) in a living animal. Yet the cochlear fluids exhibit the same mechanical properties (essentially, those of water) before and after death.

It was therefore to be expected that the other component of the mechanical system – the basilar membrane itself – would prove to have very different properties in living animals from those identified in cadavers (essentially, the properties of an isotropic elastic plate) by Békésy (1960). Soon, Voldřich (1978, 1983) uncovered those remarkably anisotropic properties (see §1) of the living basilar membrane that allow neighbouring short sections to vibrate almost independently of one another; and Lighthill (1981, 1983) indicated, using methods that had been introduced by Steele (1974, 1976) and Steele & Taber (1979), the very special importance of this discovery for the propagation of cochlear travelling waves.

Above all, those properties of the basilar membrane avoid any substantial dependence of its stiffness on the wavenumber k (whereas the local stiffness of an isotropic plate is a steeply increasing function of wavenumber because it includes a term in Gk^4, where G is its flexural rigidity). Thus the travelling wave, as its distance from the base increases, can continue to experience that decrease in stiffness which slows it down, even though, as a result, its wavenumber is becoming much bigger.

Figure 1 shows the character of the cochlear travelling waves excited on a squirrel monkey's basilar membrane by a pure tone with a sound level of 70 dB at a frequency of 2 kHz, as indicated by the classical experiments of Rhode (1971). The

waveform (distribution of basilar-membrane displacement in nanometres, as a function of position in centimetres) is plotted at one instant of time – note the transition from very long to very short waves, associated with a steep increase of amplitude preceding a precipitous fall to zero – while the envelope of the travelling wave is also given.

This paper concentrates on the waves in a region where they have become quite short, with local wavelength of about 2 mm or less, corresponding at 2 kHz to a wave speed c of at most 4 ms^{-1}. In figure 1, for example, this is the region around 1.3 cm or more from the base. We focus attention on such regions of relatively low wave speed and large amplitude because these are where (if anywhere) a formula such as (1) has at least some chance of representing a significant mean streaming velocity.

In terms of the wavenumber k, we are concerned with regions where $k \geqslant 3\ \mathrm{mm}^{-1}$. In such regions the fluid motions excited by the basilar membrane's wavelike movements may be expected to penetrate only a limited distance (of order k^{-1}) into the cochlea, being therefore uninfluenced by its external boundaries at a distance h of at least 0.6 mm away.

Here, there is a close parallel with surface waves on water of depth h which, if $kh \geqslant 1.8$, are unaffected by the bottom (see, for example, Lighthill 1978*b*, p. 217) and may be described as 'waves on deep water'. For such waves, the well-known dispersion relationship $\omega^2 = gk$ linking frequency and wavenumber can be physically interpreted (Lighthill 1978*b*, p. 213) in terms of a stiffness ρg per unit area of free surface – whose displacement ζ from its undisturbed shape is resisted by a force $\rho g\zeta$ per unit area – and an inertia ρk^{-1} per unit area associated with fluid motions penetrating a mean distance k^{-1} into the fluid; thus,

$$\omega^2 = \frac{\text{stiffness}}{\text{inertia}} = \frac{\rho g}{\rho k^{-1}} = gk. \tag{7}$$

In energy terms, the stiffness and inertia are coefficients of $\frac{1}{2}\zeta^2$ and $\frac{1}{2}(\partial\zeta/\partial t)^2$ in the potential and kinetic energies per unit area, and the relationship (7) ensures that – as in all vibrations – energy is divided equally between its kinetic and potential forms.

Despite their similarities to surface waves on deep water, cochlear travelling waves exhibit certain differences, as follows. Fluid inertia is essentially doubled, since on both sides of the basilar membrane fluid motions are excited. It is also modified, in comparison with long-crested surface waves, by the limited width of the basilar membrane, stretched between the rigid bony shelf and spiral ligament. All this means that we must speak of an inertia per unit length of basilar membrane (rather than per unit area); which should take the form

$$A\rho k^{-1} + B, \tag{8}$$

where a fluid component $A\rho k^{-1}$ (with A as a distance comparable with the basilar membrane's width) is augmented by a constant term B representing the inertia per unit length of the basilar membrane itself along with any other solid material that vibrates with it.†

† In this paper, then, we define inertia and stiffness at each cochlear cross-section as the coefficients of $\frac{1}{2}(\partial\zeta/\partial t)^2$ and $\frac{1}{2}\zeta^2$ in the kinetic and potential energies per unit length, respectively, where ζ is the basilar membrane's displacement at the point of the cross-section where displacement is greatest. (This departure from the choice, h, of generalized coordinate in Lighthill 1981, 1983, 1991 is prompted by some readers' resistance to the use of such a generalized coordinate with the dimensions of area.)

Besides inertia, both damping and stiffness are also modified. The boundary condition satisfied by fluid motions at the basilar membrane leads to the presence of Stokes boundary layers on both sides of it, producing increased damping (see §4 and Appendix A).

But by far the largest departure from (7) lies in the fact (§1) that the stiffness s of the basilar membrane, instead of taking a uniform value ρg, is a steeply falling function $s(x)$ of distance x from the base. This, with equation (8) for inertia, implies that the dispersion relationship (7) is replaced by a relationship

$$\omega^2 = \frac{s(x)}{A\rho k^{-1} + B}, \tag{9}$$

varying with position – albeit in a relatively 'smooth' manner.

Fortunately, however, general theories of waves in fluids (Lighthill 1978*b*, §4.5) show how approximate solutions of excellent accuracy may be derived for systems with a dispersion relationship varying smoothly with position. Where there is variation with just one coordinate x, such solutions are obtained from these four rules:

(*a*) at each position x, the local wavenumber k (rate of increase in phase lag with x) is given to good approximation by the dispersion relationship;

(*b*) the waveform is locally that appropriate to waves with a uniform wavenumber taking this value k;

(*c*) its amplitude varies with position as specified by the property that energy travels at the group velocity (5); and

(*d*) relative errors in these solutions are of order the square of the ratio of a relative rate of change in k (such as $k^{-1}\partial k/\partial x$) to k itself.

All of the different forms of high-frequency asymptotics – including the WKB method widely used by Steele (1974, 1976) – give identical results to these; and Steele & Taber (1979) explicitly compared them, for a 'two-dimensional' cochlear model, with a close-mesh finite-difference computation which Allen (1977) had been able to make in this case, and found extremely close agreement.

Given the dispersion relationship (9) which makes ω^{-2} a linear function of k^{-1}, we obtain the group velocity (5) in the form

$$U = \frac{\partial \omega}{\partial k} = \frac{A\rho\omega^3}{2s(x)\,k^2}. \tag{10}$$

For waves of a specified frequency ω, rule (*a*) gives the variation of k as

$$k = \frac{A\rho}{\omega^{-2}s(x) - B} = \frac{A\rho\omega^2}{s(x) - s(x_r)}, \tag{11}$$

which becomes large as x approaches x_r, that 'resonance' position (for frequency ω) where the inertia B of the basilar membrane and of other solid material that moves with it satisfies the equation

$$\omega^2 B = s(x_r). \tag{12}$$

Also, rule (*b*) implies that the local form (6) of Laplace's equation for wavenumber k governs the fluid motion outside the Stokes boundary layer; solutions of (6) appropriate to the boundary conditions are found in §3, and supplemented in §4 by calculation of the attached Stokes boundary layers and the dissipation therein.

Next, rule (*c*) implies that energy travels at a velocity U given by (10) and (11) as

$$U = \frac{[s(x)-s(x_r)]^2}{2A\rho\omega s(x)}, \tag{13}$$

an equation indicating that group velocity tends to zero like the square of the distance from $x = x_r$. This allows energy an unlimited time $\int U^{-1}\,dx$ to reach $x = x_r$; in practice, an unlimited time for dissipation to reduce it to zero (see below).

Lastly, rule (*d*) shows that the solution's relative error does not increase, despite the unlimited growth in k, but remains of order the square of the bounded quantity

$$k^{-2}\,\partial k/\partial x = -s'(x)/(A\rho\omega^2). \tag{14}$$

The approximation's continuing accuracy near $x = x_r$ is further checked in §4 by comparison with an exact solution.

Now the wave energy (potential plus kinetic) per unit length can be written

$$E = \tfrac{1}{2}s(x)\langle\zeta^2\rangle + \tfrac{1}{2}(A\rho k^{-1}+B)\langle(\partial\zeta/\partial t)^2\rangle \tag{15}$$

as just indicated in a footnote; with, moreover, the relationship (9) making equal the two terms on the right-hand side and so offering 'either term doubled' as a simplified form of E. Using the first term for this purpose and multiplying it by the group velocity given by (10) or (13), we obtain the energy flow rate in alternative forms as

$$UE = \tfrac{1}{2}A\rho\omega^3 k^{-2}\langle\zeta^2\rangle = (2A\rho\omega)^{-1}[s(x)-s(x_r)]^2\langle\zeta^2\rangle. \tag{16}$$

In the absence of dissipation, this energy flow UE would remain constant, implying that $\langle\zeta^2\rangle$ increases like k^2 and the wave amplitude like k (see (11) above) as $x \to x_r$. It is noteworthy also that the kinetic energy term

$$\tfrac{1}{2}(A\rho k^{-1}+B)\,\omega^2\langle\zeta^2\rangle \tag{17}$$

in (15) is a sum of fluid and solid kinetic energies, which both increase, but like k and k^2 respectively – the former more gradually because the energy's penetration into the fluid is falling like k^{-1}.

With D as the proportional rate of energy dissipation per unit time (to be calculated in §4 and Appendix A), the proportional diminution in energy flow between x_0 and x is

$$\frac{U(x)\,E(x)}{U(x_0)\,E(x_0)} = \exp\left(-\int_{x_0}^{x}\frac{D}{U}\,dx\right): \tag{18}$$

an equation that may perhaps be considered self-evident since energy traverses a distance dx in time dx/U; or, alternatively, demonstrated by solving the differential equation

$$DE = -\,d(UE)/dx \tag{19}$$

obtained by identifying the rate of energy dissipation in unit length with the downward gradient of energy flow. Evidently the right-hand side of (18) must become extremely small wherever (13) makes U fall to zero in such a way that the integral in (18) is increasing without limit.

Space was saved in this section by a concentration on the waves where they have become quite short ($k \geqslant 3\ \mathrm{mm}^{-1}$); however, readers will find an account of the complete progress of the waves to their characteristic place from their origin at the cochlear base in the review by Lighthill (1991) and references therein. The analogy to water waves is sustained in that review; in the region near the base, for example,

cochlear travelling waves prove to be non-dispersive and very closely analogous to 'long' waves in water channels.

Lighthill (1991) also surveys extensive recent evidence to the effect that, at low sound levels, a physiologically 'active' process (utilizing metabolic energy) applies a process of amplification by positive feedback to cochlear travelling waves. Such a process, which appears to involve the outer hair cells in stimulated vibration at audio-frequencies, would (as explained in §3 below) generate not only forward travelling waves, which could reinforce those whose energy is already 'piling up' at the characteristic place, but also backward travelling waves. The fact that these are observed (Kemp 1978, 1980), and can be shown pharmacologically to originate in an 'active' process, is part of the evidence for such a feedback phenomenon; which, furthermore, is consistent with electrophysiological observations on outer hair cells (Ashmore 1987, 1989), and explains too the very considerable peak amplitude enhancement observed (Sellick, Patuzzi & Johnstone 1982) when incident sound levels are reduced from the 70 dB of figure 1 to relatively low levels (such as 0 to 30 dB) around the threshold of hearing. Sellick *et al.* (1982) noted moreover that whenever (with the benefits of such enhancement) the velocity amplitude for basilar membrane vibration in the guineapig cochlea attained about 0.04 mm s^{-1}, neural activity was stimulated by inner hair cells.

Cochlear hair cells, indeed, are highly differentiated in mammals, with outer hair cells now believed responsible for the amplification function just described, and inner hair cells specializing in the transduction function; that is, conversion of an acoustic signal into neural activity in the attached auditory nerve fibres. There continues to be much uncertainty about the mechanism of transduction in mammalian inner hair cells, but recent observations (K. Å. I. Flock 1988, personal communication) to the effect that sustained neural activity is generated even by a steady deflection of their stereocilia suggest that it may be of value to estimate, as is attempted in this paper (§§6–9), the magnitude of such mean streaming motions as may result from the viscous dissipation of cochlear travelling waves.

3. Local distribution of wave motions around the basilar membrane

At a position in the cochlea where the wavenumber is k, the local wave motions outside Stokes boundary layers are closely approximated (§2) by solutions of equation (6) compatible with boundary conditions on the basilar membrane. Now (6) has the so-called fundamental solution

$$-(2\pi)^{-1}K_0(kr), \tag{20}$$

representing for motions of wavenumber k (assumed positive†) the velocity potential ϕ at a distance r from a source of unit strength. Here, K_0 is the modified Bessel function of the second kind, plotted in figure 2 together with its asymptotic tendencies (Watson 1944, with γ as Euler's constant 0.577)

$$K_0(kr) \sim -\log(\tfrac{1}{2}kr) - \gamma \quad \text{as} \quad kr \to 0, \quad \text{and} \quad \sim \mathrm{e}^{-kr}(\pi/2kr)^{\frac{1}{2}} \quad \text{as} \quad kr \to \infty. \tag{21}$$

Here, the first result makes the solution (20) behave for small kr like the potential, $(2\pi)^{-1}\log r + \text{constant}$, of a simple line source satisfying the two-dimensional Laplace equation; but the second result restricts to a distance hardly more than k^{-1} the penetration of the source-like motions into the external fluid.

† By contrast, if k were negative (representing waves travelling towards the base), the appropriate solution would be $-(2\pi)^{-1}K_0(|k|r)$; and, similarly, (21), (24), (25), (27) and (28) below would become valid with k either positive or negative if k were replaced by $|k|$.

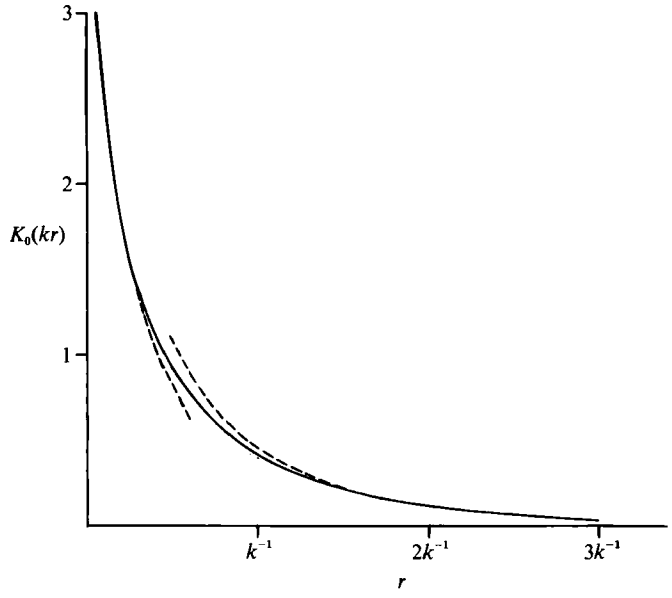

FIGURE 2. The solid line plots the modified Bessel function $K_0(kr)$ that appears in the fundamental solution (20) to equation (6), while the broken lines plot its asymptotic tendencies (21) for small and large kr respectively.

These two properties allow us to use the fundamental solution (20) to obtain a good approximation to the fluid motions generated by given vibrations of the basilar membrane. Admittedly, current knowledge of the detailed mechanical properties of the basilar membrane *in vivo* does not extend to an identification of the precise shape of its principal vibrational bending mode. Fortunately, however, we can obtain results for an arbitrarily assumed bending mode; finding, furthermore, that these results are not critically dependent on the mode chosen.

In the plane (y, z) of a cochlear cross-section where the basilar membrane extends from $z = a$ to $z = b$ on the axis $y = 0$, its vibrations with frequency ω and local wavenumber k may produce a local velocity distribution of the form

$$\partial\phi/\partial y = V(z) \quad \text{on} \quad y = 0, \quad a \leqslant z \leqslant b, \tag{22}$$

where $V(a) = V(b) = 0$ and where the complex exponential factor $e^{i(\omega t - kx)}$ has been suppressed. The corresponding potential ϕ on the side $y > 0$ can be written using the source-like solution (20) in terms of a linear distribution of sources over the strip $a \leqslant z \leqslant b$ with source strength

$$2V(z)\,dz \quad \text{in each small interval } dz, \tag{23}$$

for the following reasons:

(i) the potential of this source distribution (23) satisfies the boundary condition on the side $y > 0$ because it yields a volume flow $V(z)\,dz$ into that side (half the total output of the source) from the interval dz;

(ii) admittedly, this same source distribution (23) would yield an identical volume flow $V(z)\,dz$ into the side $y < 0$ where, on the other hand, no use is made of the potential associated with (23);

(iii) for the side $y < 0$, in fact, the corresponding fluid motion is that associated with a source strength $-2V(z)\,dz$ (there is, of course, no continuity between the fluid

motions on the two sides of the basilar membrane – whose vibrations are, indeed, driven by the difference between their pressure distributions);

(iv) the motions associated with each source (23) are directed radially outwards from it, so that they cannot interfere with the boundary condition (22) being satisfied at other points of the strip; and, lastly,

(v) the limited penetration of the source potential (20) into the fluid implies that it also avoids significantly interfering with conditions to be satisfied at the cochlear cross-section's rigid boundaries.

Accordingly, in the region specified in §2 for study in this paper (with wavenumber $k \geqslant 3\ \mathrm{mm}^{-1}$), we may utilize at points (y, z) with $y > 0$ a potential given by the distribution (23) of sources (20) as

$$\phi = -\pi^{-1} \int_a^b V(Z)\, K_0\{k[y^2 + (z-Z)^2]^{\frac{1}{2}}\}\, \mathrm{d}Z. \tag{24}$$

Among inferences from (24), the most useful of all – because it determines both the fluid velocity immediately outside the Stokes boundary layer and, with (22), the kinetic energy of the fluid motions – is a specification of the limit of ϕ as $y \to 0$ (from above) as

$$(\phi)_{y=0} = -\pi^{-1} \int_{-\infty}^{\infty} V(Z)\, K_0(k\,|Z-z|)\, \mathrm{d}Z; \tag{25}$$

where the integral's limits can be redesignated as shown if, by convention, $V(Z)$ is taken as zero outside $a \leqslant Z \leqslant b$ (being assumed, moreover, to join smoothly on to that value at the ends of the strip). The integral (25) can be asymptotically estimated by expanding $V(Z)$ in a Taylor series

$$V(Z) = \sum_{m=0}^{\infty} V^{(m)}(z)\, \frac{(Z-z)^m}{m!} \tag{26}$$

of which only the terms with m even (say, $m = 2n$) make any contribution to the integral (25). Using the expression (Watson 1944, p. 388)

$$\int_{-\infty}^{\infty} K_0(k\,|Z-z|)\, \frac{(Z-z)^{2n}}{(2n)!}\, \mathrm{d}Z = \pi k^{-2n-1}\, \frac{1.3 \ldots (2n-1)}{2.4 \ldots (2n)}, \tag{27}$$

we can derive the asymptotic behaviour of (25) as

$$(\phi)_{y=0} \sim -k^{-1}V(z) - \tfrac{1}{2}k^{-3}V''(z) - \tfrac{3}{8}k^{-5}V''''(z) - \cdots. \tag{28}$$

Here the leading term, which is

$$\phi \sim -k^{-1}V(z), \quad \text{yielding} \quad \partial\phi/\partial x = -\mathrm{i}k\phi \sim +\mathrm{i}V(z), \quad \partial\phi/\partial z \sim -k^{-1}V'(z) \tag{29}$$

as local velocity components – along with (22) for $\partial\phi/\partial y$ – just outside the Stokes boundary layer, may often be a close enough approximation. Then the x- and y-components of velocity, with their equal amplitudes $V(z)$ and 90° phase difference, represent a classical circular motion (as in waves on deep water) about some axis $z =$ constant. For large enough k this dominates the fluid motions in the neighbourhood of the basilar membrane, motions which we shall then describe as 'locally two-dimensional' (albeit with a z-dependent amplitude). When k is not so large, however, the presence of a significant z-component of velocity $-k^{-1}V'(z)$ tilts the plane of motion through an angle $\tan^{-1}(k^{-1}V'/V)$; and there are possibilities of additional terms in the asymptotic series (28) becoming significant.

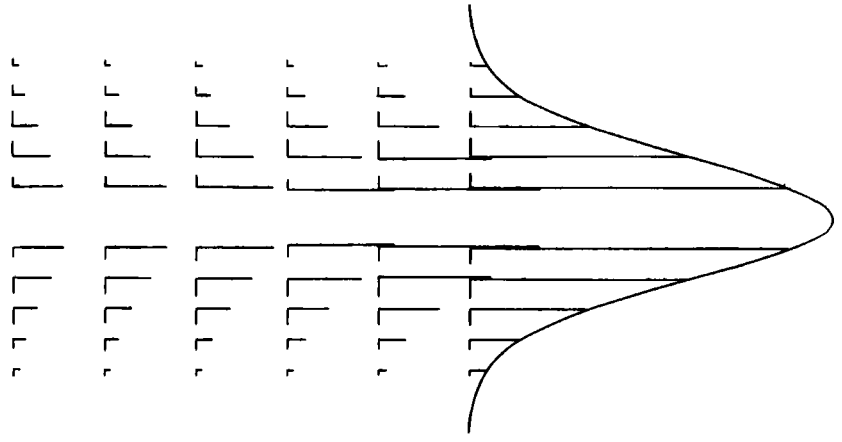

FIGURE 3. The trend to locally two-dimensional motion near the 'resonance' position $x = x_r$ is illustrated, using the first two terms of the asymptotic series (28), by showing the amplitudes of $\partial\phi/\partial x$ (horizontal lines) and $\partial\phi/\partial z$ (vertical lines) at six locations with values of $s(x)-s(x_r)$ in the ratios (left to right) 6:5:4:3:2:1. According to (11) and (16), the wavenumber k changes as the reciprocal of these differences, and so does the scale of $V(z)$ in the region before the onset of substantial energy dissipation. In this diagram a somewhat arbitrary choice of principal bending mode (distribution of $V(z)$ across the width of the basilar membrane – see the right-hand curve) was unavoidably made.

Figure 3 shows the trend towards a 'locally two-dimensional' motion, as k increases in accordance with (11), for a somewhat arbitrarily chosen bending mode (to whose shape, however, such results are not particularly sensitive), by indicating the direction and amplitude of the tangential fluid velocities just outside the Stokes boundary layer, as derived from the first two terms in the asymptotic series (28). It is in the right-hand region (the region where both k and V are largest) that streaming motions are most likely to be significant, which is why streaming will first be calculated (§6) for locally two-dimensional motions – although generalized results for three-dimensional motions are given in §7.

The excess or 'transient' pressure may be written

$$-\rho\,\partial\phi/\partial t = -\rho i\omega\phi, \tag{30}$$

which is in its expected ratio $\rho\omega k^{-1} = \rho c$ to the fluid velocity component $\partial\phi/\partial x$ in the direction of propagation. An excess pressure equal and opposite to (30) acts on the side $y < 0$ of the basilar membrane, whose y-component of velocity $V(z)$, then, is excited by a pressure difference $+2\rho i\omega\phi$.

In the asymptotic limit (29) this is $(-2\rho k^{-1})$ times the local acceleration $i\omega V(z)$. From the standpoint of the theory of elasticity we can, in this limit, describe the basilar membrane's principal bending mode $V(z)$ as that which would be associated with 'free vibrations' such as are simply resisted by inertial forces proportional to local acceleration, where, however, the effective mass per unit area of basilar membrane is locally augmented by a fluid inertia term $2\rho k^{-1}$.

At a time such as $t = 0$ when the complex exponential suppressed in (22) takes the value 1, the kinetic energy of the fluid in the region $y > 0$ can be derived, by use of a general theorem of irrotational-flow theory, as

$$-\tfrac{1}{2}\rho\int_a^b (\phi\,\partial\phi/\partial y)_{y=0}\,\mathrm{d}z = -\tfrac{1}{2}\rho\int_a^b (\phi)_{y=0}\,V(z)\,\mathrm{d}z \tag{31}$$

per unit length of cochlea, and the total kinetic energy of fluid (in the regions $y > 0$ and $y < 0$) is twice as much. This, on the approximation (29), gives a value

$$2\rho k^{-1} \int_a^b \tfrac{1}{2}[V(z)]^2 \, \mathrm{d}z, \tag{32}$$

which, once again, is consistent with the effective mass per unit area of basilar membrane being directly augmented by a fluid inertia term $2\rho k^{-1}$.

But improvements to the expression (32) for kinetic energy can be calculated by using also the second term in the asymptotic series (28). In this case, after an integration by parts, we obtain

$$2\rho k^{-1} \int_a^b \tfrac{1}{2}[V(z)]^2 \, \mathrm{d}z - \rho k^{-3} \int_a^b \tfrac{1}{2}[V'(z)]^2 \, \mathrm{d}z \tag{33}$$

for the kinetic energy of fluid at a time such as $t = 0$. This completely general indication (33) of a reduction below the asymptotic value (32) as k decreases is consistent with all calculations of fluid inertia that have been made in particular cases (Lighthill 1981, 1983).

In the notation of §2 with the fluid kinetic energy as

$$\tfrac{1}{2}(\partial\zeta/\partial t)^2 A\rho k^{-1}, \tag{34}$$

where ζ is the maximum displacement of the basilar membrane, we can see that $\partial\zeta/\partial t = V_{\max}$ (the largest value of V) and therefore that

$$A \sim 2V_{\max}^{-2} \int_a^b [V(z)]^2 \, \mathrm{d}z. \tag{35}$$

This result is, of course, consistent with the idea (§2) that A would be comparable with the width $(b–a)$ of the basilar membrane.

The corresponding kinetic energy of the basilar membrane itself and of other solid material attached to it – with, say, a combined mass per unit area $M(z)$ – may be written

$$\int_a^b \tfrac{1}{2}M(z) \, [V(z)]^2 \, \mathrm{d}z. \tag{36}$$

This takes, as in §2, the form $\frac{1}{2}B(\partial\zeta/\partial t)^2$ provided that

$$B = V_{\max}^{-2} \int_a^b M(z) \, [V(z)]^2 \, \mathrm{d}z. \tag{37}$$

Similarly, in order that the potential energy shall take the form $\frac{1}{2}s(x)\zeta^2$, we find that $s(x)$ must take the form

$$s(x) = V_{\max}^{-2} \int_a^b S(x, z) \, [V(z)]^2 \, \mathrm{d}z, \tag{38}$$

where $S(x, z)$ is the ratio of restoring force per unit area to basilar-membrane displacement.

We now conclude this section with a brief analysis of the consequences of basilar-membrane forcing by vibrations of outer hair cells. Such forcing may be expected to be effective in augmenting the principal mode $V(z)$ of vibration of the basilar membrane provided that the z-distribution of force applied to the membrane has a normal-mode expansion (in terms of basilar-membrane vibrational modes) with a

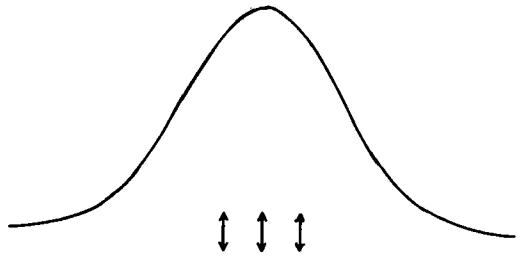

FIGURE 4. Illustrating how the principal bending mode used in figure 3 would be excited preferentially by in-phase vibrations of outer hair cells because all are located around this mode's maximum (whereas higher bending modes would have nodes in the neighbourhood of at least one of them).

rather substantial principal-mode component. We immediately verify this suggestion, whose importance lies in the fact that, at a cross-section where the three outer hair cells vibrate in phase (figure 4), their principal-mode component is expected to dominate.

For pure-tone forcing

$$e^{i\omega t} f(x, z) \tag{39}$$

in the y-direction, with amplitude $f(x, z)$ per unit area, we write

$$f(x, z) = \int_{-\infty}^{\infty} e^{-ikx} F_1(k, z)\, dk \tag{40}$$

so that $F_1(k, z)$ is the Fourier transform of f with respect to x. On substitution in (39), equation (40) gives a distribution of forcing terms which, on suppression of the complex exponential $e^{i(\omega t - kx)}$ as in the earlier part of this section, take the form

$$F_1(k, z). \tag{41}$$

Now, in the region (near the characteristic place) where forcing is expected to be important, the potential ϕ may be approximated by its locally two-dimensional form (29); then that difference in the pressure (30) which acts alongside the forcing (41) to generate the basilar membrane's motions is

$$-2\rho i\omega |k|^{-1} V(z), \tag{42}$$

an equation whose validity (see footnote at the beginning of §3) has been made independent of the sign of k through its replacement by $|k|$. The forcing terms (41) and (42) taken together must generate the motion of the basilar membrane and attached solid material, with mass $M(z)$ and local stiffness $S(x, z)$, giving

$$M(z) i\omega V(z) + S(x, z)\, (i\omega)^{-1} V(z) = F_1(k, z) - 2\rho i\omega |k|^{-1} V(z). \tag{43}$$

Moreover, (43) after multiplication by $V(z)$ and integration from a to b can be simplified, using (35), (37) and (38), to

$$V_{\max}^2 [(A\rho |k|^{-1} + B) i\omega + (i\omega)^{-1} s(x)] = \int_a^b F_1(k, z)\, V(z)\, dz. \tag{44}$$

Accordingly, with

$$F(k) = V_{\max}^{-1} \int_a^b F_1(k, z)\, V(z)\, dz, \tag{45}$$

and $i\omega\zeta = V_{\max}$ (as before), the forcing equation becomes

$$[s(x)-\omega^2(A\rho|k|^{-1}+B)]\zeta = F(k). \tag{46}$$

Equation (46) confirms both that unforced waves satisfy the dispersion equation (11), and that forcing of the principal mode $V(z)$ depends on $F(k)$, whose expression (45) relates it to the principal-mode component of $F_1(k,z)$.

In addition to those 'unforced' waves that travel from the base of the cochlea towards their characteristic place, the 'forced' waves newly generated by the forcing (39) may be propagated either in the same or in the opposite direction. A very familiar technique derives these forced waves in a simple homogeneous-system case with s constant. Then, for forcing as in (39) and (40) by a continuous distribution of terms in $e^{i(\omega t-kx)}$, equation (46) specifies the resulting basilar-membrane vibration as

$$\zeta = e^{i\omega t}\int_{-\infty}^{\infty}\frac{F(k)\,e^{-ikx}\,dk}{s-\omega^2(A\rho|k|^{-1}+B)}, \tag{47}$$

and the waves generated may be derived by Cauchy's theorem in terms of the poles of the integrand (values of k for which the denominator in (47) vanishes) satisfying 'the radiation condition' that energy must travel outwards from the source region (see Lighthill 1978*b*, for example).

The pole $+k_0$ (the positive wavenumber for which the dispersion relationship (11) is satisfied for s constant) yields waves travelling away from the source region in the apical direction (x increasing), specified by Cauchy's theorem as

$$\zeta = -2\pi i\,e^{i(\omega t-k_0x)}\,k_0^2F(k_0)/(\omega^2A\rho); \tag{48}$$

here, the factor k_0^2 shows us that forcing produces responses which are resonantly intensified near the characteristic place (where the dispersion relationship makes the wavenumber large). On the other hand, the negative pole $-k_0$ yields waves travelling away form the source region in the basal direction (x decreasing), specified as

$$\zeta = -2\pi i\,e^{i(\omega t+k_0x)}\,k_0^2F(-k_0)/(\omega^2A\rho). \tag{49}$$

These latter waves (49) may be described as 'evoked otoacoustic emissions': basally travelling waves generated in response to an acoustic signal when it stimulates vibrations of outer hair cells. On this simplified theory (with s taken as constant), the entire difference between the amplitudes of the waves (48) travelling apically and (49) travelling basally lies in the factors $F(k_0)$ and $F(-k_0)$ respectively. These are important differences, however, which throw light on why only certain regions of the cochlea generate evoked otoacoustic emissions of significant magnitude.

Indeed, wherever outer hair cells are organized so that each responds to the ambient travelling-wave signal, proportional to $e^{i(\omega t-k_0x)}$, with approximately the same phase lag, then the value of k for which (40) defines a substantial Fourier transform $F_1(k,z)$, so that (45) similarly makes $F(k)$ substantial, must be centred around $k = k_0$. Under such circumstances, the apically travelling forced wave (48) with the $F(k_0)$ factor must dominate, and the basally travelling forced wave (49) must (owing to the $F(-k_0)$ factor) be relatively insignificant.

By contrast, imperfections of organizations of outer-hair-cell responses can inhibit any such concentration of substantial values of $F(k)$ around $k = k_0$. Accordingly, in any region where such imperfections occur, $F(-k_0)$ may be significant so that evoked otoacoustic emissions may be substantial, with a rate (16) of energy flow in the basally travelling wave equal to

$$\pi^2k_0^2|F(-k_0)|^2/(\omega A\rho). \tag{50}$$

The preliminary over-simplified description of cochlear forced waves which has just been derived for the homogeneous-system case s = constant can very crudely be extended to the real case of a cochlea with $s(x)$ variable by the usual assumptions of high-frequency asymptotics. Then as the wave (49) travels basally, its originally generated energy flow (50) should proceed without significant change as the wavenumber k falls gradually from its value k_0 near the position of forcing to those very low values that it takes near the base, where in turn that energy flow might be assumed to be transmitted through the middle ear's linkage mechanism into the outer ear canal and observed as an otoacoustic emission.

For the apically travelling wave, furthermore, a similar approach might perhaps be attempted, but for the fact that this wave propagates alongside the main 'unforced' wave travelling from the base towards its characteristic place. The forced wave, given by (48) on the over-simplified assumption s = constant, must of course undergo increases in the wavenumber k above the value k_0 taken near the position of forcing, while being supplemented by an unforced wave undergoing the same changes. Provided that they are approximately in phase, they should reinforce one another. No detailed attempt to analyse this process is made here, however, both because details of the forcing applied by outer hair cells remain unknown, and because the present paper is one that concentrates its attention upon mean streaming motions. In the streaming context, the relevant property of the wave amplification by positive feedback associated with outer-hair-cell forcing is that it may allow amplitude-dependent streaming motions, such as may be given for example by (1), to become significant near the characteristic place.

4. Locally two-dimensional motions and their Stokes boundary layers

Figure 3 illustrates the strong tendency, associated with unlimited increase in the wavenumber k as the characteristic place is approached, for cochlear travelling waves to become locally two-dimensional. We now consider further, both for 'unforced' and for 'forced' waves, the nature of such locally two-dimensional motions, and of the related thin Stokes boundary layers – attached to the basilar membrane – within which all vorticity fluctuations are expected to be confined.

In any locally two-dimensional flow the irrotational motions outside the Stokes boundary layer satisfy the simplified form

$$\partial^2\phi/\partial y^2 - k^2\phi = 0 \tag{51}$$

of (6). The correspondingly simplified boundary condition

$$\partial\phi/\partial y = V \quad \text{on} \quad y = 0 \quad (\text{for } V \text{ constant}) \tag{52}$$

represents the local form of (22) for a particular value of z (with the complex exponential $e^{i(\omega t - kx)}$ again suppressed).

On the side $y > 0$ of the basilar membrane, (51) subject to the boundary condition (52) has the solution

$$\phi = -k^{-1}V e^{-ky}, \tag{53}$$

which, in addition, may be shown to be the asymptotic form of (25) for large k. The corresponding x-velocity,

$$u = \partial\phi/\partial x = +iV e^{-ky}, \tag{54}$$

satisfies the local form of condition (29) on $y = 0$ and, in combination with a y-velocity

$$v = \partial\phi/\partial y = V e^{-ky}, \tag{55}$$

describes the well-known circular motions of particles characteristic of waves on deep water (Lighthill 1978*b*, figure 50) as well as of cochlear travelling waves near their characteristic place (Lighthill 1981, figure 4*a*).

Before proceeding with any further use of these locally two-dimensional solutions for particular large values of the wavenumber k – solutions which, of course, the principles (*a*)–(*d*) of high-frequency asymptotics (§2) allow us to apply to travelling waves of continuously varying wavenumber – we may reasonably ask for an independent verification of the correctness of such an approach. An interesting exact solution of the two-dimensional Laplace equation conveniently provides this in the case of unforced (and undissipated) waves near the characteristic place.

This is a region where (11) leads us to expect a wavenumber increase like

$$k \sim N(x_r - x)^{-1}, \quad \text{where} \quad N = A\rho\omega^2[-s'(x_r)]^{-1} \tag{56}$$

is a non-dimensional constant. Accordingly, the definition (4) of wavenumber as rate of increase of phase lag of basilar-membrane oscillations with distance x from the base suggests, asymptotically, that

$$\text{phase lag} \sim -N \log (x_r - x) + \text{constant}, \tag{57}$$

while (16) makes us expect the wave amplitude to increase like the wavenumber.

These properties are completely consistent with those of a simple exact solution of the Laplace equation for two-dimensional irrotational flow:

$$\phi = C e^{i\omega t}(x_r - x + iy)^{iN}, \tag{58}$$

whose value on the basilar membrane $y = 0$ may be written

$$C \exp \{i[\omega t + N \log (x_r - x)]\} \tag{59}$$

in exact agreement with (57). The velocity components on the basilar membrane are

$$\partial\phi/\partial x = -iN\phi(x_r - x)^{-1} \quad \text{and} \quad \partial\phi/\partial y = -N\phi(x_r - x)^{-1}, \tag{60}$$

confirming similarly that their amplitudes vary like $(x_r - x)^{-1}$ as does k, and also that their phases differ by 90° as do those of the expressions (54) and (55) for the approximate solution (53). Finally, that approximate solution agrees with the form of (58) for small values of $y/(x_r - x)$ when it can be written

$$\phi = (\phi)_{y=0}\{\exp [iy(x_r - x)^{-1}]\}^{iN} = (\phi)_{y=0} e^{-ky}, \tag{61}$$

with k given by its asymptotic form (56).

These are valuable confirmations of the conclusions of §2 that principles (*a*)–(*d*) give a good account of cochlear travelling waves (and, in particular, that principle (*d*) assures their accuracy even where k becomes very large); checking these conclusions explicitly for undissipated waves by comparison with an exact solution which (because the waves are undissipated) builds up at $x_r = x, y = 0$ to a formidable 'singularity'. Confirmation in this case encourages us to use those principles also in other, more realistic cases with viscous dissipation (and indeed with forcing), founding our analysis on the continued use of locally two-dimensional solutions.

Viscous dissipation takes place, of course, in thin Stokes boundary layers incorporating that vorticity which, after being generated at the solid surface, diffuses away from it with diffusivity $\mu/\rho = \nu$ (the kinematic viscosity). Vorticity generation arises because, although the boundary condition (52) specifying the y-velocity on the basilar membrane is sufficient by itself to determine a unique solution (53) of the equation (51) governing irrotational flow, nevertheless the fluid motions must

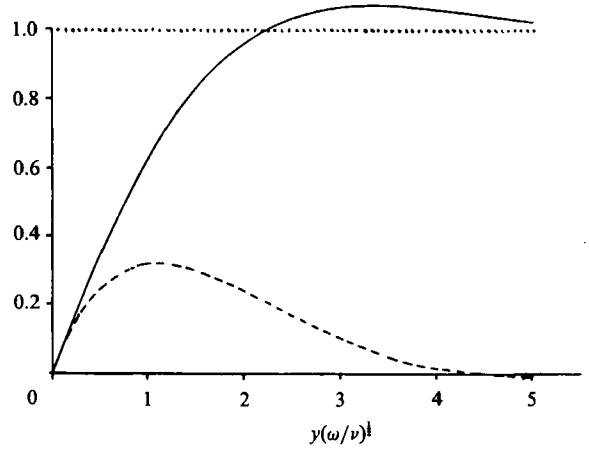

FIGURE 5. The Stokes boundary layer: an oscillatory motion parallel to a solid boundary is modified at small distances y from the wall by the factor given in curly brackets in (63), whose real and imaginary parts are the solid line (with asymptote 1, the dotted line) and the broken line, respectively. Note how the vorticity (gradient of the velocity distribution) shows a phase lag which increases with distance from the boundary.

comply also with a second boundary condition constraining the x-component of velocity to be zero on the solid surface. Any discontinuity between the irrotational-flow value (54) of that x-velocity and this true value (zero) constitutes, of course, a vortex sheet; and one whose strength oscillates with frequency ω while the vorticity in the sheet diffuses outwards.

Oscillatory quantities subject to such diffusion acquire a characteristic distribution proportional to

$$\exp\left[-y(\mathrm{i}\omega/\nu)^{\frac{1}{2}}\right], \tag{62}$$

which, with distance from the boundary, falls off exponentially in magnitude while its phase lag continually increases. The general character of velocity distributions within Stokes layers (figure 5) is consistent with these suggestions that any vorticity remaining at relatively larger distances from the solid surface has been generated at relatively earlier phases of the cycle.

In the present problem, with the x-velocity (54) just outside the thin boundary layer given as $u = \mathrm{i}V$, its distribution across the boundary layer takes the form

$$u = \mathrm{i}V\{1-\exp\left[-y(\mathrm{i}\omega/\nu)^{\frac{1}{2}}\right]\} \tag{63}$$

of a rotational motion with the required distribution (62) of vorticity which allows the boundary condition $u = 0$ on $y = 0$ to be satisfied. The corresponding y-velocity v, with its boundary value V on $y = 0$, is derived from (63) by the equation of continuity as

$$v = V[1+(1-\exp\left[-y(\mathrm{i}\omega/\nu)^{\frac{1}{2}}\right])\, k(\nu/\mathrm{i}\omega)^{\frac{1}{2}}]. \tag{64}$$

The rate of energy dissipation Δ per unit area of boundary layer takes the form

$$\Delta = \int_0^\infty \mu(\tfrac{1}{2}|\partial u/\partial y|^2)\,\mathrm{d}y, \tag{65}$$

where the quantity in brackets is the mean-square shear rate in the velocity distribution (63). The integral (65) is readily evaluated as

$$\Delta = \rho V^2(\tfrac{1}{8}\omega\nu)^{\frac{1}{2}}. \tag{66}$$

For cochlear travelling waves, of course, this indicates the energy dissipation rate in either of the two boundary layers attached to the basilar membrane, and the overall rate is twice as much.

All the standard boundary-layer approximations have been used in the above determination of the velocity distributions (63) and (64) within the Stokes layer and of the energy dissipation rate (66). These approximations require, of course, that the boundary-layer scale $(\nu/\omega)^{\frac{1}{2}}$ is small compared with scale k^{-1} of the external irrotational flow, or in other words that the non-dimensional wavenumber

$$\kappa = k(\nu/\omega)^{\frac{1}{2}} \tag{67}$$

is small. They additionally necessitate meticulous care in making use, along classical lines, of those Stokes-layer distributions against the background of the external irrotational motions (54) and (55). Several such calculations are made in §§5 and 6.

The approach used could be made more rigorous, of course, by the method of matched asymptotic expansions. A preferable alternative, here adopted in Appendices A, B and C, gives a rigorous verification of all our results for small κ and also extends them to arbitrarily chosen values of κ. For example, Appendix A determines uniformly valid velocity fields for all values of κ and calculates the exact energy dissipation rate Δ, checking that, for κ small, Δ is indeed given to good approximation by its Stokes-layer value (66).

5. The distinction between Euler and Lagrange mean flows

The rest of this paper is concerned with estimating the mean streaming motions generated by cochlear travelling waves. It must be recognized at the outset, therefore, that two alternative definitions of mean motion need to be carefully distinguished. To this end, subscripts E and L are used to designate, respectively, the Euler mean motion (average velocity at a fixed point in space) and the Lagrange mean motion (average velocity for a particle of fluid).

The importance of this distinction has been stressed by McIntyre (see for example Andrews & McIntyre 1978), so it is appropriate to use the subscript M for the difference (3) between the Lagrange mean velocity and the Euler mean velocity. The present section is devoted exclusively to a calculation of this difference for the locally two-dimensional motions of §4.

In the waves (53) outside the Stokes boundary layer – identical to waves on deep water – the difference takes a well-established value

$$u_{\mathrm{M}} = k\omega^{-1}V^2\,\mathrm{e}^{-2ky}, \quad v_{\mathrm{M}} = 0 \tag{68}$$

known as the Stokes drift. Integrating (68) from 0 to ∞, we obtain the net Stokes drift as

$$\int_0^\infty u_{\mathrm{M}}\,\mathrm{d}y = \tfrac{1}{2}\omega^{-1}V^2. \tag{69}$$

Here the upper limit ∞ really represents the extent of penetration (of order k^{-1}) of wave motions into the fluid, and the integral (69) gives the net mass flow (per unit width of the basilar membrane, on the side $y > 0$) associated with the waves outside the Stokes layer in any case when the Euler mean motion is zero.

The results (68) are obtained for the oscillatory motions (54) and (55) – where the complex exponential $\mathrm{e}^{\mathrm{i}(\omega t - kx)}$ has been suppressed so that the motions as they stand have zero Euler mean – by writing down oscillatory particle displacements δx and δy as

$$\delta x = u/(\mathrm{i}\omega), \quad \delta y = v/(\mathrm{i}\omega) \tag{70}$$

and determining the Lagrange mean velocity u_L for a particle as

$$u_L = \langle (\partial u/\partial x)\,\delta x + (\partial u/\partial y)\,\delta y \rangle. \tag{71}$$

Then, using the rule that the average value of the product of two quantities specified as the real parts of complex multiples of $e^{i\omega t}$ is half the real part of the product of one quantity with the complex conjugate of the other, we can calculate (71) as

$$\tfrac{1}{2}\,\mathrm{Re}\,[(-ik)\,u\bar{u}/(-i\omega) - ku\bar{v}/(-i\omega)] = \tfrac{1}{2}\,\mathrm{Re}\,[k\omega^{-1}V^2 e^{-2ky} + k\omega^{-1}V^2 e^{-2ky}], \tag{72}$$

while a similar calculation of v_L shows it to be zero – a result which, indeed, follows for arbitrary waveform from the continuity equation $\partial v/\partial y = iku$. Thus, when the velocity field is taken to have zero Euler mean, the Lagrange mean is found to have the value (68), which, furthermore, becomes the difference (u_M, v_M) between the Lagrange and Euler means when the same mean velocity field (u_E, v_E) as a function of position in space is added on to both.

A similar calculation inside the Stokes boundary layer uses the same general results (70) and (71) but with (63) and (64) specifying u and v. Then the rule quoted after (71) gives

$$\begin{aligned} u_M &= \tfrac{1}{2}\,\mathrm{Re}\,[(-ik)\,u\bar{u}/(-i\omega) + (\partial u/\partial y)\bar{v}/(-i\omega)] \\ &= \tfrac{1}{2}\,\mathrm{Re}\left\{k\omega^{-1}V^2\,|1-\exp\,[-y(i\omega/\nu)^{\frac{1}{2}}]|^2 + \left[iV\exp\,[-y(i\omega/\nu)^{\frac{1}{2}}]\left(\frac{i\omega}{\nu}\right)^{\frac{1}{2}}\right]\frac{V}{-i\omega}\right. \\ &\quad \left.\times\left[1+(1-\exp\,[-y(-i\omega/\nu)^{\frac{1}{2}}])\,k\left(\frac{\nu}{-i\omega}\right)^{\frac{1}{2}}\right]\right\}. \end{aligned} \tag{73}$$

The right-hand side of (73) is interesting because every term but one exhibits exactly the same scaling (like $k\omega^{-1}V^2$) as the value (68) of u_M outside the boundary layer. Specifically, every term but one can be written as $k\omega^{-1}V^2$ times a function of the Stokes-layer coordinate $y(\omega/\nu)^{\frac{1}{2}}$, and these terms all taken together change smoothly from zero at $y = 0$ to a value at the edge of the layer of $k\omega^{-1}V^2$ consistent with the value of (68) for small y.

The exceptional term in (73) – with very strongly contrasting properties – is the term

$$-\tfrac{1}{2}\mathrm{Re}\left[\omega^{-1}V^2\exp\,[-y(i\omega/\nu)^{\frac{1}{2}}]\left(\frac{i\omega}{\nu}\right)^{\frac{1}{2}}\right] \tag{74}$$

arising from the element 1 within the last large square bracket. This term takes a negative value at the wall,

$$(u_M)_{y=0} = -\frac{V^2}{(8\nu\omega)^{\frac{1}{2}}}, \tag{75}$$

which represents the actual value of u_M because the other terms add up to zero for $y = 0$. Furthermore, the contribution to $\int_0^\infty u_M\,dy$ made by this term (74) is

$$-\tfrac{1}{2}\omega^{-1}V^2, \tag{76}$$

which exactly cancels out the net Stokes drift (69). Such cancellation is rendered possible by the enhanced magnitude of the reverse flows in the Stokes layer, with their peak value (75) reflecting the maximum transverse displacements $V/(i\omega)$ at the wall acting on the maximum gradient of the Stokes-layer velocity distribution (63).

In summary, one very famous property of waves on deep water – the net Stokes drift of particles in the direction of wave propagation – is nullified for cochlear

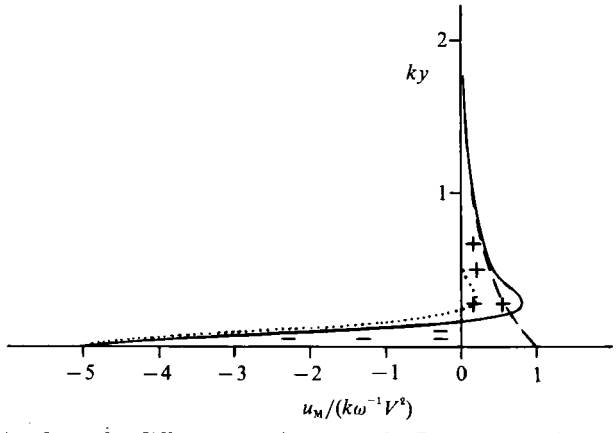

FIGURE 6. Illustrating how the difference u_M between the Lagrange and Euler mean flows makes a transition (equation (B 13): solid line) between (68) for the Stokes drift (broken line) outside the Stokes boundary layer and a very different form (74) within it (dotted line), in such a way that (79) holds (zero net mass flow). Here, the non-dimensional wavenumber (67) has been taken as $\kappa = 0.07$.

travelling waves by an equal and opposite net flow within the Stokes boundary layer. The above analysis, to be sure, suggests only that they cancel to first order on the usual boundary-layer approximations. Appendix B demonstrates, however, that the cancelling is exact for all values of κ, the non-dimensional wavenumber (67), and that this exact cancellation persists even when the wavenumber k takes complex values representing waves with spatial growth or decay.

I am indebted to Dr M. E. McIntyre for the following general argument explaining why the cancellation must be exact. The expression (71) for u_L can be rewritten as a divergence

$$u_L = \partial\langle u\delta x\rangle/\partial x + \partial\langle u\delta y\rangle/\partial y \tag{77}$$

because the vector field $\delta\boldsymbol{r} = (\delta x, \delta y)$ given by (70) is necessarily solenoidal. Now the divergence theorem

$$\int_V u_L \,\mathrm{d}V = \int_{\partial V} \langle u\delta\boldsymbol{r}\rangle \cdot \boldsymbol{n}\,\mathrm{d}S \tag{78}$$

applied to the volume V between two closely adjacent parallel planes $x =$ constant includes on the right-hand side

(*a*) zero contributions over the planes themselves, where $\langle u\delta\boldsymbol{r}\rangle \cdot \boldsymbol{n} = \pm\langle u\delta x\rangle$ with this mean value $\langle u\delta x\rangle$ vanishing because u and δx, by (70), are 90° out of phase;

(*b*) another zero contribution from the basilar membrane itself where $u = 0$; and

(*c*) just one more contribution, also zero, from a boundary at great distances, where disturbances tend to zero.

Therefore the left-hand side of (78) is also zero, which implies a zero integral of u_L with respect to y.

These conclusions much reduce the potential importance of any Stokes-drift element for acoustic streaming in the cochlea. Figure 6 indicates how apically directed particle movements (designated +, with $u_M > 0$) are balanced by basally directed movements (designated −, with $u_M < 0$). The solid line represents the exact calculation of Appendix B, satisfying

$$\int_0^\infty u_M \,\mathrm{d}y = 0, \tag{79}$$

while the broken and dotted lines represent the approximate forms of u_M outside the boundary layer (broken line) and inside it.

There is just one further context in which the distinction between Euler and Lagrange mean flows is important. The boundary condition on the mean x-velocity at the solid boundary $y = 0$ takes the form $u_L = 0$ because the x-velocity of a fluid particle on the vibrating basilar membrane must be zero at all times – so that its mean u_L is zero. The boundary condition on u_E can therefore be written down, using (75), as

$$(u_E)_{y=0} = -(u_M)_{y=0} = +\frac{V^2}{(8\nu\omega)^{\frac{1}{2}}}, \tag{80}$$

a form used in §6 for the determination of mean flows forced by gradients of Reynolds stresses.

6. Forcing by Reynolds stresses

Although, in cochlear travelling waves, excess mass flows are locally balanced, exhibiting equal and opposite flows outside and inside the Stokes boundary layer which (together) are rather ineffective for generating mean streaming motions, no such local balance appears in the (more powerful) excess momentum flows. Their forcing effects, operative only inside the Stokes layer, are studied in §6 for the locally two-dimensional motions of §4.

Reynolds (1896) pointed out that the mean rate of momentum flow across unit area is effectively a force per unit area; that is, a stress – now known as the Reynolds stress. In two-dimensional motions, for example, the Reynolds stress component $\rho\langle uv\rangle$ acts as a shear stress, transferring x-momentum in the y-direction (across unit area); and the consequent rate of increase in x-momentum (inflow *minus* outflow) per unit volume is

$$-\rho\frac{\partial}{\partial y}\langle uv\rangle, \tag{81}$$

being able to generate what we shall call 'shear-stress streaming'.

In addition, a Reynolds stress component $\rho\langle u^2\rangle$ acts as a normal stress, transferring x-momentum in the x-direction; so that a resulting rate of increase in x-momentum per unit volume,

$$-\rho\frac{\partial}{\partial x}\langle u^2\rangle, \tag{82}$$

may generate 'normal-stress streaming'. However, in the special case of travelling waves whose amplitude V is independent of x, the normal stress $\rho\langle u^2\rangle$ must also be independent of x so that the associated forcing (82) is zero. Accordingly, in this special case (which we analyse first), only shear-stress streaming is found.

Outside the boundary layer, moreover, the velocity components u and v are given by (54) and (55) which are 90° out of phase, so that the Reynolds shear stress $\rho\langle uv\rangle$ is zero. Forcing occurs, therefore, only in the thin Stokes boundary layer, where it generates an Euler mean flow in the form of a thin vortex sheet, allowing a steep change in the Euler mean velocity u_E from its value at $y = 0$ given by the boundary condition (80) to its value at the edge of the Stokes layer (where forcing disappears).

At any particular point within the Stokes layer, the rate $\rho\langle uv\rangle$ of inflow of momentum (per unit area) might in principle be partly balanced by an outflow

$\rho\langle uv\rangle_{\text{edge}}$ at the edge of the layer; which, although it vanishes in the inviscid limit, may be non-zero to the next approximation of boundary-layer theory. Then the net inflow $\rho\langle uv\rangle - \rho\langle uv\rangle_{\text{edge}}$ of momentum into the intervening fluid must be balanced by the viscous stress $\mu\partial u_{\text{E}}/\partial y$ acting within the steady Euler-mean-flow vortex sheet. This gives a very simple differential equation

$$\partial u_{\text{E}}/\partial y = \nu^{-1}(\langle uv\rangle - \langle uv\rangle_{\text{edge}}) \tag{83}$$

for the Euler mean flow, and the solution satisfying the boundary condition (80) can be written

$$u_{\text{E}} = \frac{V^2}{(8\nu\omega)^{\frac{1}{2}}} + \nu^{-1}\int_0^y (\langle uv\rangle - \langle uv\rangle_{\text{edge}})\,\mathrm{d}y. \tag{84}$$

It is above all the value of u_{E} at the edge of the Stokes layer which represents the net effect of shear stress forcing in producing a flow external to the layer. This value may be written

$$u_{\text{S}} = \frac{V^2}{(8\nu\omega)^{\frac{1}{2}}} + \nu^{-1}\int_0^\infty (\langle uv\rangle - \langle uv\rangle_{\text{edge}})\,\mathrm{d}y, \tag{85}$$

with the upper limit ∞ representing the edge of the layer (where the integrand is zero). Essentially, u_{S} represents a boundary value (often described in the acoustic-streaming literature as an effective 'slip velocity') for that low-Reynolds-number Euler mean motion outside the boundary layer which is given initial study in §9 below.

We calculate u_{S} using (63) and (64) for the velocity components u and v inside the Stokes layer; then the rule quoted after (71) gives

$$\begin{aligned}\langle uv\rangle &= \tfrac{1}{2}\,\mathrm{Re}\left\{\mathrm{i}V(1-\exp\left[-y(\mathrm{i}\omega/\nu)^{\frac{1}{2}}\right])\,V\left[1+(1-\exp\left[-y(-\mathrm{i}\omega/\nu)^{\frac{1}{2}}\right])\,k\left(\frac{\nu}{-\mathrm{i}\omega}\right)^{\frac{1}{2}}\right]\right\}\\ &= \tfrac{1}{2}V^2\left\{\mathrm{Re}\,(-\mathrm{i}\exp\left[-y(\mathrm{i}\omega/\nu)^{\frac{1}{2}}\right]) - |1-\exp\left[-y(\mathrm{i}\omega/\nu)^{\frac{1}{2}}\right]|^2\,k\left(\frac{\nu}{2\omega}\right)^{\frac{1}{2}}\right\}.\end{aligned} \tag{86}$$

Then the integral term in (85) can be written as the sum of two terms,

$$\nu^{-1}\int_0^\infty (\langle uv\rangle - \langle uv\rangle_{\text{edge}})\,\mathrm{d}y = -\frac{V^2}{(8\nu\omega)^{\frac{1}{2}}} + \frac{V^2 k}{4\omega}, \tag{87}$$

of which the latter comes from the last term within the curly brackets of (86); whereas the former comes from the first, and hence from the initial term 1 inside the square brackets of (64).

Equation (87) implies that the shear-stress streaming (85) takes a value

$$u_{\text{S}} = \tfrac{1}{4}V^2 k\omega^{-1} \tag{88}$$

identical with that calculated in classical acoustic-streaming theory for the interaction of travelling sound waves with a rigid wall. At first sight this may seem quite a surprising 'coincidence', because cochlear travelling waves – with the wall vibrating, and with particles in circular motions outside the Stokes layer – are so different from plane sound waves.

Inside the Stokes layer, however, the velocity components (63) and (64) differ from those in sound waves propagating along a rigid wall in but one respect: their inclusion in (64) of the first term, 1, in square brackets. This produces (§5) the

additional term (74) in u_M, leading to the boundary condition (80) on u_E. Now we see also that the same term generates on the right-hand side of (87) an exactly cancelling expression! – whilst the other terms, present in both theories, lead to the same formula (88) for u_S in each and thus to the apparent coincidence.

The same considerations, analogously, make quite unnecessary any separate calculation of the contribution to u_S, in motions when the velocity amplitude V may be varying with x, from the normal-stress forcing (82), since this depends solely on the velocity component u – with the same Stokes-layer distribution in both theories. Exactly as in classical acoustic-streaming theory, then, normal-stress forcing makes a contribution

$$-\tfrac{1}{2}V(\mathrm{d}V/\mathrm{d}x)\omega^{-1} \tag{89}$$

to u_S; see also Appendix C for a comprehensive calculation which derives without making any boundary-layer approximation the corresponding result for all values of κ, the non-dimensional wavenumber (67), and proves too that the Stokes-layer result (89) is a correct limiting value for κ small.

Both for sound waves and for cochlear travelling waves, moreover, an additional contribution

$$-\tfrac{1}{4}V(\mathrm{d}V/\mathrm{d}x)\omega^{-1} \tag{90}$$

is made to shear-stress streaming in cases when the velocity amplitude V is varying with x. This contribution arises from the extra term

$$\mathrm{i}\frac{\mathrm{d}V}{\mathrm{d}x}\left[-y+(1-\exp\left[-y(\mathrm{i}\omega/\nu)^{\frac{1}{2}}\right])\left(\frac{\nu}{\mathrm{i}\omega}\right)^{\frac{1}{2}}\right] \tag{91}$$

in the Stokes-layer form of v which the equation of continuity then requires in both theories, and which, with (63) for u, adds a contribution (90) to the equation (85) for u_S. For a demonstration that our Stokes-layer results for shear-stress streaming are a correct small-κ limit of results not making any boundary-layer approximation, see Appendix B.

The three results (88), (89) and (90) for different components of u_S, the streaming velocity forced by Reynolds stresses acting within the Stokes layer, may be combined into a single equation

$$u_S = \tfrac{1}{4}V^2 k\omega^{-1} - \tfrac{3}{4}V(\mathrm{d}V/\mathrm{d}x)\,\omega^{-1}. \tag{92}$$

This equation, representing the effective 'slip velocity' at the boundary for the Euler mean motions external to the boundary layer, extends the classical acoustic-streaming result (1) to cochlear travelling waves – justifying, perhaps, this paper's title 'Acoustic streaming in the ear itself'.

7. Modifications to streaming formulae for three-dimensional motions

The streaming results in §§5 and 6 were derived for the locally two-dimensional motions of §4, which are expected to be an increasingly good approximation in those regions, very near the characteristic place, where (if anywhere) streaming motions may possibly be important. This consideration – along with a current lack of accurate knowledge about basilar-membrane bending modes – might be thought to imply that any extension of streaming formulae to three-dimensional motions would at present be premature; nevertheless, in a paper aiming to offer a comprehensive account of how mean streaming motions may be estimated for cochlear travelling waves, it seems advisable to put such modifications on record.

There is moreover, within the entire literature of acoustic streaming, a regrettable absence of information about streaming generated within three-dimensional Stokes boundary layers. The present section, then, may be seen as going part of the way towards filling that gap by showing how the appropriate treatment proceeds in one important case (that of cochlear travelling waves). At the same time, readers who may prefer to skip this section can rest assured that they will not thereby be hampered in studying later sections!

The calculations are presented for a three-dimensional Stokes boundary layer where the x-velocity u and the z-velocity w just outside it take values

$$u = \mathrm{i}V \quad \text{and} \quad w = W. \tag{93}$$

As in §6, the streaming is calculated first of all in the simple case when V and W are constants (independent of x and z), after which any effects of their spatial non-uniformity (variation with x and z) on generating additional streaming motions are determined. In the meantime, we recall that (29) suggests

$$W = -k^{-1}\,\partial V/\partial z \tag{94}$$

as a useful approximation near the characteristic place to the value of w just outside the Stokes layer.

Inside the layer, the expression (63) for u is complemented by a similar expression

$$w = W(1-\exp\,[-y(\mathrm{i}\omega/\nu)^{\frac{1}{2}}]) \tag{95}$$

for w. Here, it is noteworthy that u and w remain 90° out of phase for all values of y. This simplifies streaming theory because it makes one particular Reynolds stress component vanish:

$$\rho\langle uw\rangle = 0. \tag{96}$$

In the case to be considered initially (with V and W as constants) there is no $\partial w/\partial z$ term in the equation of continuity, which, accordingly, yields (64) for v as before. Then the difference w_{M} between the z-velocity's Lagrange and Euler means can be written

$$w_{\mathrm{M}} = \langle(\partial w/\partial x)\,\mathrm{d}x + (\partial w/\partial y)\,\delta y\rangle, \tag{97}$$

which, inside the Stokes layer, takes the form

$$w_{\mathrm{M}} = \tfrac{1}{2}\,\mathrm{Re}\,[-\mathrm{i}kw\bar{u}/(-\mathrm{i}\omega) + (\partial w/\partial y)\bar{v}/(-\mathrm{i}\omega)]. \tag{98}$$

Here, however, (96) makes the first term in square brackets vanish; while the second term gives

$$w_{\mathrm{M}} = \tfrac{1}{2}\,\mathrm{Re}\left\{\left[W\exp\,[-y(\mathrm{i}\omega/\nu)^{\frac{1}{2}}]\left(\frac{\mathrm{i}\omega}{\nu}\right)^{\frac{1}{2}}\right]\frac{V}{-\mathrm{i}\omega}\left[1-ky\right.\right.$$
$$\left.\left.+(1-\exp\,[-y(-\mathrm{i}\omega/\nu)^{\frac{1}{2}}])\,k\left(\frac{\nu}{-\mathrm{i}\omega}\right)^{\frac{1}{2}}\right]\right\}. \tag{99}$$

This equation, in sharp contrast to (73), makes w_{M} tend to zero outside the layer (where no z-component of mass flow accompanies the Stokes drift in the x-direction). Its leading term inside the layer is

$$\tfrac{1}{2}\,\mathrm{Re}\left[\mathrm{i}\omega^{-1}WV\exp\,[-y(\mathrm{i}\omega/\nu)^{\frac{1}{2}}]\left(\frac{\mathrm{i}\omega}{\nu}\right)^{\frac{1}{2}}\right], \tag{100}$$

arising like (74) from the element 1 within the last square bracket. At $y = 0$, where indeed the other terms vanish, this term (100) takes a negative value

$$(w_{\mathrm{M}})_{y=0} = -\frac{WV}{(8\nu\omega)^{\frac{1}{2}}} \tag{101}$$

analogous to (75); on the other hand, the contribution to $\int_0^\infty w_{\mathrm{M}}\,\mathrm{d}y$ made by this term (100) is zero. There is, in short, zero mass flow in the z-direction both outside and inside the boundary layer, so that the conclusions of §5 about the ineffectiveness of excess mass flows for generating streaming remain unchanged.

Forcing by Reynolds stresses, in the special case of constant V and W, is due entirely to shear stresses. At any particular point within the Stokes layer, the rate $\rho\langle vw\rangle$ of inflow of z-momentum (per unit area) may be partly balanced, as in §6, by a rate $\rho\langle vw\rangle_{\mathrm{edge}}$ of outflow at the edge of the layer, and it is their difference that must in turn be balanced by a viscous shear stress $\mu\partial w_{\mathrm{E}}/\partial y$ acting within the steady Euler-mean-flow vortex sheet. Therefore, the differential equation (83) for u_{E} is replaced by one for w_{E} of a similar form

$$\partial w_{\mathrm{E}}/\partial y = \nu^{-1}(\langle vw\rangle - \langle vw\rangle_{\mathrm{edge}}), \tag{102}$$

which must be solved subject to the boundary condition

$$(w_{\mathrm{E}})_{y=0} = -(w_{\mathrm{M}})_{y=0} = \frac{WV}{(8\nu\omega)^{\frac{1}{2}}}. \tag{103}$$

Then the value of w_{E} at the edge of the layer becomes

$$w_{\mathrm{S}} = \frac{WV}{(8\nu\omega)^{\frac{1}{2}}} + \nu^{-1}\int_0^\infty (\langle vw\rangle - \langle vw\rangle_{\mathrm{edge}})\,\mathrm{d}y. \tag{104}$$

Here, from (64) and (95) for v and w, we have

$$\langle vw\rangle = \tfrac{1}{2}\,\mathrm{Re}\left\{W(1-\exp\,[-y(\mathrm{i}\omega/\nu)^{\frac{1}{2}}])\,V\left[1+(1-\exp\,[-y(-\mathrm{i}\omega/\nu)^{\frac{1}{2}}])\,k\left(\frac{\nu}{-\mathrm{i}\omega}\right)^{\frac{1}{2}}\right]\right\} \tag{105}$$

so that

$$\langle vw\rangle - \langle vw\rangle_{\mathrm{edge}} = \tfrac{1}{2}WV\left\{-\mathrm{Re}\,\exp\,[-y(\mathrm{i}\omega/\nu)^{\frac{1}{2}}] + (|\,1-\exp\,[-y(\mathrm{i}\omega/\nu)^{\frac{1}{2}}]|^2 - 1)\,k\left(\frac{\nu}{2\omega}\right)^{\frac{1}{2}}\right\}. \tag{106}$$

The integral of (106) from 0 to ∞ can be written as the sum of two terms

$$-\frac{VW}{(8\nu\omega)^{\frac{1}{2}}} - \frac{VWk}{4\omega} \tag{107}$$

corresponding, as with (87), to the main terms in (106), but with their values significantly modified because the $\mathrm{i}V$ in (63) for u has been replaced by the W in (95) for w. Nevertheless the net effect on the component (104) of shear-stress streaming is an equation

$$w_{\mathrm{S}} = -\tfrac{1}{4}WVk\omega^{-1} \tag{108}$$

very closely parallel to (88) for u_{S}.

Next, as in §6, we study in two parts the effects of spatial variability of wave amplitudes. First, we consider normal-stress streaming, obtaining the same contribution

$$-\tfrac{1}{2}V(\partial V/\partial x)\,\omega^{-1} \tag{109}$$

as before (see (89) above) to the x-component u_S from forcing by the x-gradient of the Reynolds stresses $\rho\langle u^2\rangle$. The corresponding forcing by the z-gradient of the Reynolds stress component $\rho\langle w^2\rangle$ makes an exactly analogous contribution

$$-\tfrac{1}{2}W(\partial W/\partial z)\,\omega^{-1} \tag{110}$$

to w_S.

Secondly, we must find the additional shear-stress streaming in cases when the velocity amplitudes V and W may vary with x and z. Then the equation of continuity constrains us to include in the Stokes-layer form of v an extra term

$$\left(\mathrm{i}\frac{\partial V}{\partial x}+\frac{\partial W}{\partial z}\right)\left[-y+(1-\exp\left[-y(\mathrm{i}\omega/\nu)^{\frac{1}{2}}\right])\left(\frac{\nu}{\mathrm{i}\omega}\right)^{\frac{1}{2}}\right], \tag{111}$$

slightly more complicated than (91). With (63) for u, this adds on to $\langle uv\rangle$ a term

$$\tfrac{1}{2}\,\mathrm{Re}\left\{\mathrm{i}V(1-\exp\left[-y(\mathrm{i}\omega/\nu)^{\frac{1}{2}}\right])\left(-\mathrm{i}\frac{\partial V}{\partial x}+\frac{\partial W}{\partial z}\right)\left[-y+(1-\exp\left[-y(-\mathrm{i}\omega/\nu)^{\frac{1}{2}}\right])\left(\frac{\nu}{-\mathrm{i}\omega}\right)^{\frac{1}{2}}\right]\right\}. \tag{112}$$

Accordingly, $\langle uv\rangle-\langle uv\rangle_{\mathrm{edge}}$ is changed by a term

$$\begin{aligned}\tfrac{1}{2}\,\mathrm{Re}\left\{V\left(\frac{\partial V}{\partial x}+\mathrm{i}\frac{\partial W}{\partial z}\right)\right.&\left[\exp\left[-y(\mathrm{i}\omega/\nu)^{\frac{1}{2}}\right]\left(y-\left(\frac{\nu}{-\mathrm{i}\omega}\right)^{\frac{1}{2}}\right)\right.\\&\left.\left.-(1-\exp\left[-y(\mathrm{i}\omega/\nu)^{\frac{1}{2}}\right])\exp\left[-y(-\mathrm{i}\omega/\nu)^{\frac{1}{2}}\right]\left(\frac{\nu}{-\mathrm{i}\omega}\right)^{\frac{1}{2}}\right]\right\}\end{aligned} \tag{113}$$

so that its integral from 0 to ∞ is changed by

$$\tfrac{1}{2}\,\mathrm{Re}\left\{V\left(\frac{\partial V}{\partial x}+\mathrm{i}\frac{\partial W}{\partial z}\right)\left[\frac{\nu}{\mathrm{i}\omega}-\frac{\nu}{\omega}-\frac{\nu}{-\mathrm{i}\omega}+\frac{\nu}{\omega(-2\mathrm{i})^{\frac{1}{2}}}\right]\right\}=-\tfrac{1}{4}\nu V\frac{\partial V}{\partial x}\omega^{-1}+\tfrac{3}{4}\nu V\frac{\partial W}{\partial z}\omega^{-1}, \tag{114}$$

and yields a contribution to u_S, by (85), of

$$-\tfrac{1}{4}V\frac{\partial V}{\partial x}\omega^{-1}+\tfrac{3}{4}V\frac{\partial W}{\partial z}\omega^{-1}. \tag{115}$$

The analogous contribution to (104) for w_S is obtained from a form of $\langle uv\rangle$ which is (112) with the initial factor $\mathrm{i}V$ replaced by W, so that on the left-hand side of (114) the initial factor V is replaced by $-\mathrm{i}W$. This yields a contribution

$$-\tfrac{1}{4}W\frac{\partial W}{\partial z}\omega^{-1}-\tfrac{3}{4}W\frac{\partial V}{\partial z}\omega^{-1} \tag{116}$$

to w_S.

The different contributions (88), (109) and (115) to u_S, and similarly the contributions (108), (110) and (116) to w_S, may now be combined to give as the final conclusions of the three-dimensional streaming analysis

$$\left.\begin{aligned}u_S&=\tfrac{1}{4}V^2k\omega^{-1}-\tfrac{3}{4}V(\partial V/\partial x-\partial W/\partial z)\,\omega^{-1},\\ w_S&=-\tfrac{1}{4}WVk\omega^{-1}-\tfrac{3}{4}W(\partial W/\partial z+\partial V/\partial x)\,\omega^{-1}.\end{aligned}\right\} \tag{117}$$

Any apparent asymmetry in these conclusions is, of course, merely a consequence of the 90° phase difference between the 'edge' values (93) of the x- and z-velocities.

Near the characteristic place, we can make the substitution (94) to obtain a first approximation to the magnitude of these three-dimensional effects. This gives

$$\left.\begin{aligned} u_S &= \tfrac{1}{4}V^2 k\omega^{-1} - \tfrac{3}{4}V(\partial V/\partial x + k^{-1}\partial^2 V/\partial z^2)\,\omega^{-1}, \\ w_S &= \tfrac{1}{4}V(\mathrm{d}V/\mathrm{d}z)\,\omega^{-1} + \tfrac{3}{4}(\partial V/\partial z)\,(\partial V/\partial x - k^{-1}\partial^2 V/\partial z^2)\,k^{-1}\omega^{-1}, \end{aligned}\right\} \tag{118}$$

equations which indicate how the x-component of the streaming motion may be modified by a k^{-1} term while the motion also acquires a z-component independent of k. These are modifications of only moderate magnitude which it will, perhaps, be unnecessary to take into account in initial estimates of streaming.

8. Modifications to streaming formulae for high wavenumbers

For cochlear travelling waves, this paper's central conclusion is that forcing by Reynolds stresses in Stokes boundary layers (§6) produces mean streaming motions near the characteristic place that are described approximately by (92), in essential agreement with (1) for classical acoustic streaming as analysed by Rayleigh (1896). This conclusion of §6 has already been critically examined from two points of view: the possibility that 'Stokes drift' might contribute significantly to streaming has been scrutinized (§5) and largely discounted, while modifications due to three-dimensional effects have just been worked out (§7) and shown in (118) to be significant only at relatively lower wavenumbers. We now embark on a third critique, concerned with how far (92) retains its validity at very high wavenumbers k, when the boundary-layer approximation breaks down because the Stokes layer ceases to be thin on the lengthscale k^{-1} of penetration of wave motions into the cochlear fluids.

The compelling need for all this critical analysis – and for its detailed exposure to expert and discerning readers of the *Journal of Fluid Mechanics* – derives from the practical impossibility of experimentally measuring mean streaming motions in any living cochlea. This implies that only by a scrupulously careful estimation process – founded on well-established principles of biophysics, biomechanics and above all fluid mechanics – is there any chance of assessing whether or not mean streaming motions may possibly be mediating inner-hair-cell transduction in the immediate neighbourhood of the characteristic place. Because, moreover, this location is where the greatest wavenumbers are expected to be found, the previous calculations must be repeated for values of κ, the non-dimensional wavenumber (67), exceeding those small values for which the boundary-layer approximation may be justifiable.

These are the considerations which necessitated the quite extensive analysis set out in Appendices A, B and C. On the other hand, that analysis without any use of the boundary-layer approximation has saved much space in §6, where simple application of the approximation on classical lines led quickly to the basic equation (92), without any substantiation by 'matching' methods being called for, because the Appendices prove this equation to be a rigorous small-κ limit.

Here, we simply indicate the method pursued in the Appendices and set out the principal results. The method uses (Appendix A) the full Navier–Stokes equations for a viscous incompressible fluid and determines small-amplitude solutions of any

given wavenumber k, large enough for the motions to be locally two-dimensional and to satisfy boundary conditions $u = 0$, $v = V$ on $y = 0$. These two-dimensional solutions (A 4), uniformly valid for all values of κ, exhibit limiting tendencies as follows:

(i) for small κ, they show the familiar transition from boundary-layer forms (63) and (64) to the circular motions (54) and (55) outside the boundary layer; while

(ii) for large κ, they tend to forms

$$u = \mathrm{i}Vky\,\mathrm{e}^{-ky}, \quad v = V(1+ky)\,\mathrm{e}^{-ky}, \tag{119}$$

with reduced magnitude for the x-component u (see figure 11; its greatest value is only $V\mathrm{e}^{-1}$ compared with a maximum of V for the y-component v).

The solutions are valid not only for real but also for complex k, the latter case offering a convenient local representation of waves with spatial growth or decay.

The rest of Appendix A calculates the rate of energy dissipation, Δ per unit area of basilar membrane, for the flow on either side of it. Figure 12 displays how Δ makes a transition between its small-κ form (66) and a limiting form μkV^2 for large κ.

Appendix B first obtains u_{M}, the difference (3) between the Lagrange and Euler mean motions. For all values (including complex values) of k it demonstrates exactly the property (79) which was thoroughly discussed in §5.

Forcing by Reynolds stresses is then investigated. Appendix B addresses first the calculation of shear-stress streaming in waves with V independent of x; confirming the correctness of (88) for small κ but showing how, with increasing κ, shear-stress streaming rises to double that value.

Next, the case of V varying with x is treated by altering k into $k+\mathrm{i}\epsilon$ so that

$$V\mathrm{e}^{\mathrm{i}(\omega t-kx)} \quad \text{becomes} \quad V\mathrm{e}^{\epsilon x}\,\mathrm{e}^{\mathrm{i}(\omega t-kx)}. \tag{120}$$

Thus, ϵ can be used to represent $V^{-1}\,\mathrm{d}V/\mathrm{d}x$, and a calculated contribution to shear-stress streaming proportional to $V^2\epsilon$ becomes one proportional to $V\,\mathrm{d}V/\mathrm{d}x$, with (90) as its small-κ limit although with a change of sign as κ increases.

Finally, Appendix C investigates normal-stress streaming for general κ. Expressions for the rate of vorticity generation in the Euler mean motion are used to relate the strength of the vortex sheet on the basilar membrane to a difference $\rho\langle u^2-v^2\rangle$ of normal stresses. Here, $\langle v^2\rangle$ replaces a term in classical acoustic-streaming theory which is the value of $\langle u^2\rangle$ at the edge of the Stokes boundary layer. The two coincide in the small-κ limit, when both yield (89) for the normal-stress streaming; but alterations in the relative magnitude of u and v (referred to earlier) cause this contribution to u_{S}, rather like that just mentioned, to suffer a change of sign as κ increases.

At the end of Appendix C, the different contributions to u_{S} are combined into a single formula (C 26), representing a modification of our basic equation (92) for wavenumbers so high that the non-dimensional wavenumber κ is no longer small. This equation,

$$u_{\mathrm{S}} = \tfrac{1}{4}V^2k\omega^{-1}\sigma(\kappa) - \tfrac{3}{4}V(\mathrm{d}V/\mathrm{d}x)\,\omega^{-1}\tau(\kappa), \tag{121}$$

incorporates the two functions of κ plotted in figure 7. As mentioned already, the first term – a shear-stress streaming independent of $\mathrm{d}V/\mathrm{d}x$ – carries a coefficient $\sigma(\kappa)$ which doubles its value for large κ. By contrast, the second term, which combines normal-stress streaming with the component of shear-stress streaming which depends on $\mathrm{d}V/\mathrm{d}x$, carries a coefficient $\tau(\kappa)$ that exhibits an early change of sign (present in both component parts) but tends to zero for large κ.

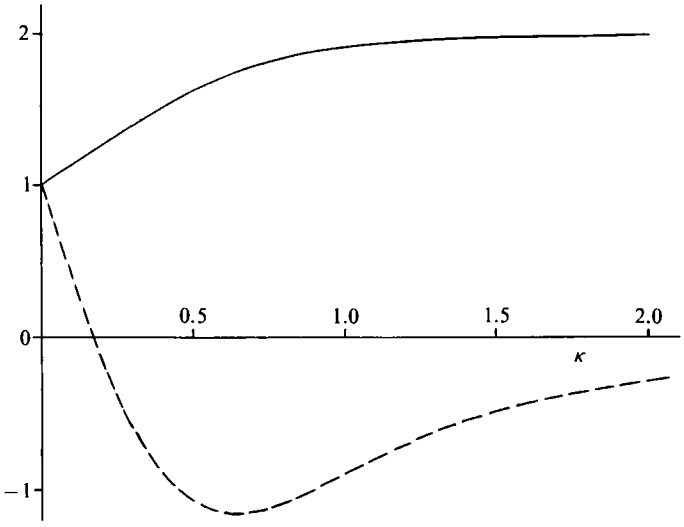

FIGURE 7. The classical acoustic-streaming formula (92) assumes for high wavenumbers the modified form (121), incorporating two functions – $\sigma(\kappa)$ (solid line) and $\tau(\kappa)$ (broken line) – of the non-dimensional wavenumber (67).

This third tranche of critical analysis of (92), then, has led to a particularly important result, in its revelation of the need, at very high wavenumbers, for some substantial modifications to that equation. These amount to a doubling of the leading term, alongside some diminution in the other term's relative importance.

If, in the large-κ limit, we ask for the physical significance of the doubled leading term, we discover that it comes entirely from the boundary condition analogous to (80),

$$(u_{\mathrm{E}})_{y=0} = -(u_{\mathrm{M}})_{y=0} = \tfrac{1}{2}V^2 k\omega^{-1}, \tag{122}$$

since the limiting equations (119) give, with $\delta y = v/(\mathrm{i}\omega)$,

$$(u_{\mathrm{M}})_{y=0} = \langle(\partial u/\partial y)\,\delta y\rangle_{y=0} = -\tfrac{1}{2}V^2 k\omega^{-1}, \tag{123}$$

while making the shear stress $\rho\langle uv\rangle$ everywhere zero. This, then, is a limiting case in which the Euler mean motions are forced entirely by the boundary condition $u_{\mathrm{L}} = 0$ on the Lagrange mean motions.

9. Mean flow across inner-hair-cell stereocilia

The aim of all the research outlined in this paper is an estimation of the magnitude of any mean motion across the row of inner-hair-cell stereocilia that may be capable of acting on them with a mean deflecting force. In this section we apply the results of our extended investigation of u_{S} – the effective slip velocity very near the basilar membrane – to estimate the mean flow pattern at locations farther away from it, such as those of inner hair cells.

From among the two kinds of mean motion distinguished in §5, we study in the first place the Euler mean motion as determined by the boundary value, u_{S}, of its x-component. Later, we consider effects of any z-component w_{S} (as estimated in §7), and address also the difficult question of whether the mean deflecting force on

stereocilia responds more to the Euler or to the Lagrange mean motion (the differences between them, however, being much reduced at the locations of inner hair cells).

It is the z-component w_E of the Euler mean motion which may be capable of exerting such a mean deflecting force. First of all, then, we must ask whether an x-component u_S of slip velocity at the basilar membrane can generate any substantial z-component w_E of mean flow across the row of inner-hair-cell stereocilia.

The simple answer is that, primarily, this may result from any abrupt change of u_S with x, as we now explain qualitatively before giving detailed fluid-mechanical calculations that support the suggestion. Both the qualitative and quantitative analyses are based on consideration of those (inertialess) 'creeping' motions in the scala media that may be generated through viscous traction by the motion u_S present at one of its boundaries.

Suppose, for example, that (as (121) may suggest) the value of u_S increases just before the characteristic place to a peak from which it falls abruptly to zero, thus producing an inflow to the characteristic place that is not matched by any outflow beyond it. In the low-Reynolds-number hydrodynamics of creeping motions, with inertia negligible, the unbalanced inflow cannot continue in any 'jet-like' form but must spread out in all directions, with, moreover, some preference for directions away from the resistive solid boundary. Within a cochlear cross-section, the part of this flow that is 'inwardly' directed – towards the inner hair cells – is available to apply an 'inward' deflecting force to their stereocilia. Indeed, a 'channelling' of flow across the row of stereocilia may result from certain features (such as the arch of Corti) of that cross-section's geometry.

The essential idea of this qualitative analysis may first of all be substantiated by a quantitative model, founded on simple physical ideas, which meticulously reflects the fluid mechanics near the basilar membrane itself although it leaves out any such special geometrical features of the scala media. It is based on an exact solution of the equations of low-Reynolds-number hydrodynamics which, besides satisfying a boundary condition

$$u = u_S(x, z), \quad v = w = 0 \tag{124}$$

on the plane $y = 0$ representing the basilar membrane, portrays a fluid flow that fills the entire region $y > 0$ – although at speeds decreasing with distance from that limited area of basilar membrane where u_S takes significant values.

This preliminary solution describes, then, how the creeping motions in the scala media are initiated at the basilar membrane. Evidently, however, modifications due to geometrical features of structures in and around the organ of Corti need to be incorporated in later analyses.

Creeping motions satisfy the linearized momentum and continuity equations

$$\nabla p = \mu \nabla^2 \boldsymbol{u}, \quad \nabla \cdot \boldsymbol{u} = 0, \tag{125a, b}$$

which omit all inertia terms (differing in this way from the equations (A 1) that govern audio-frequency motions) so that pressure gradients and viscous forces are in balance. The divergence of this balance result gives

$$\nabla^2 p = 0, \tag{126}$$

and it follows that (125a) can always be satisfied by the velocity field

$$\boldsymbol{u} = \frac{p\boldsymbol{r}}{2\mu}, \quad \text{where} \quad \boldsymbol{r} = (x, y, z) \tag{127}$$

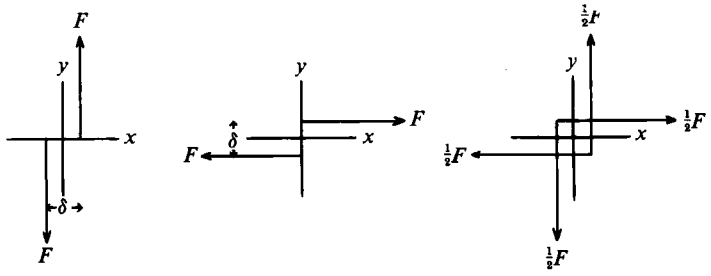

FIGURE 8. As our primary interpretation of the quadrupole pressure field (129) we use the pair of dipoles (*a*), representing forces $+F$ and $-F$ in the y-direction with (anticlockwise) moment $F\delta = Q$. Later, we note alternative interpretations: (*b*) in terms of forces $+F$ and $-F$ in the x-direction with equal and opposite moment $-Q$, and (*c*) as the mean of both configurations (a distribution of forces with zero net moment – as in the action of a shear stress).

is the position vector.

In general, however, the convenient solution (127) for (125*a*) fails to satisfy (125*b*), because

$$\nabla\cdot(p\boldsymbol{r}) = p\nabla\cdot\boldsymbol{r}+\boldsymbol{r}\cdot\nabla p = 3p+\boldsymbol{r}\cdot\nabla p \tag{128}$$

is not necessarily zero. Nevertheless, (128) is zero whenever p, besides satisfying Laplace's equation (126), is a homogeneous function of degree (-3).

One example of such a homogeneous harmonic of degree (-3) is the quadrupole pressure field

$$p = Q\left(-\frac{\partial}{\partial x}\right)\frac{y}{4\pi r^3} = Q\frac{3xy}{4\pi r^5} \tag{129}$$

associated with two equal and opposite dipole pressure fields

$$p = \frac{Fy}{4\pi r^3} \tag{130}$$

centred (figure 8) upon points a distance δ apart, where $F\delta = Q$. Acousticians know well that the dipole pressure field (130) represents the action of a force F in the y-direction concentrated at the origin; and this may be verified by calculating the resultant pressure

$$\int_{-\infty}^{\infty} p\,\mathrm{d}x\,\mathrm{d}z = \tfrac{1}{2}Fy\,|y|^{-1} \tag{131}$$

over any plane $y =$ constant – which comes to $\frac{1}{2}F$ for $y > 0$ and $-\frac{1}{2}F$ for $y < 0$, the difference between them accounting for the concentrated force F acting at $y = 0$. The pair of dipoles illustrated in figure 8 represents similarly a force-couple or torque of moment Q about the z-axis, as we may analogously verify for the pressure field (129) by calculating the moment of those pressures acting on any plane $y =$ constant:

$$\int_{-\infty}^{\infty} xp\,\mathrm{d}x\,\mathrm{d}z = \tfrac{1}{2}Qy\,|y|^{-1} = \pm\tfrac{1}{2}Q \quad \text{for} \quad y \gtrless 0, \tag{132}$$

where the difference of Q accounts for the concentrated couple or torque acting at $y = 0$.

Note that in both cases – dipole or quadrupole – the pressure field (130) or (129) is

zero at all points on $y = 0$ except the origin (where it is singular). This simply reflects the concentration of the force or couple at the origin.

Because the pressure field (129) is homogeneous of degree (-3), the velocity field (127) satisfies all the equations of motion. Also, its x-component is

$$u = \frac{px}{2\mu}, \tag{133a}$$

so that, by (132),

$$\int_{-\infty}^{\infty} u \, dx \, dz = \frac{Q}{4\mu} \quad \text{on any plane} \quad y = \text{constant} > 0. \tag{133b}$$

This result, with the fact that, as $y \to 0$ from above, u (like p) becomes zero at all points except the origin, specifies the boundary value of u as

$$u_S = \frac{Q}{4\mu} \delta(x) \, \delta(z) \tag{134}$$

where $\delta(x)$ is the Dirac delta function.

By taking $Q = 4\mu$, then, we obtain from (129) and (127) that singular solution

$$p = \frac{3\mu xy}{\pi r^5}, \quad u = \frac{3x^2 y}{2\pi r^5}, \quad v = \frac{3xy^2}{2\pi r^5}, \quad w = \frac{3xyz}{2\pi r^5} \tag{135}$$

of (125) for $y > 0$ which satisfies the boundary condition (124) with

$$u_S = \delta(x) \, \delta(z), \tag{136}$$

representing traction by a slip motion concentrated at the origin with unit integrated strength. We shall, of course, use this singular solution to write down the general solution satisfying the boundary condition (124) for arbitrary $u_S(x, z)$.

Before doing so, we comment a little further on the attractively simple solution (135). This has been described as a 'stresslet' in the literature of low-Reynolds-number hydrodynamics (Happel & Brenner 1965); and indeed, as figure 8 shows, the quadrupole form of p could equally be associated with a pair of dipoles directed at right angles, of moment $-Q$; or, alternatively, with the mean of both configurations (forces in the y-direction forming a couple of moment $\frac{1}{2}Q$ together with forces in the x-direction forming one of moment $-\frac{1}{2}Q$). Actually, the fluid motion (135) can (rather cumbersomely) be derived as the limit of the sum of four 'stokeslet' fields, one being generated by each of this 'stress-like' combination of forces. In the present application, however, the physically simpler derivation of its properties that has been given above can reasonably be preferred.

Among the velocity components in the 'stresslet' solution (135) the z-component w concerns us most since it is in the direction needed to deflect inner-hair-cell stereocilia. Although vanishing, of course, at the resistive solid boundary $y = 0$, its value in the region $y > 0$ of the scala media involve an outflow (w having the same sign as z) at all points $x > 0$ distal to the origin where slip, according to (136), is concentrated.

For a quite general distribution (124) of boundary slip, the corresponding value of w can be built up as a continuous distribution

$$w = \frac{3}{2\pi} \int_{-\infty}^{\infty} \int_{-\infty}^{\infty} \frac{(x-X) \, y (z-Z)}{[(x-X)^2 + y^2 + (z-Z)^2]^{\frac{5}{2}}} u_S(X, Z) \, dX \, dZ \tag{137}$$

of stresslet solutions (135) centred at all positions (X, Z) on the basilar membrane where slip is present. Equation (137) becomes particularly useful after an integration by parts, giving

$$w = \frac{1}{2\pi}\int_{-\infty}^{\infty}\int_{-\infty}^{\infty} \frac{y(z-Z)}{[(x-X)^2+y^2+(z-Z)^2]^{\frac{3}{2}}}\left(-\frac{\partial u_S}{\partial X}\right) dX\, dZ. \tag{138}$$

The expected pattern of multidirectional outflow from a region of unbalanced inflow such as may accompany any extremely abrupt fall of u_S from its peak value to zero is well exhibited in (138), which (where, once again, $y > 0$) ascribes to any positions (X, Z) with very high values of $(-\partial u_S/\partial X)$ an outflow (w and $(z-Z)$ having the same sign) that decays initially as just the inverse first power of distance. (Such gradual initial decay would be maintained until distances were reached where opposing contributions from proximal regions where $\partial u_S/\partial X$ takes positive – albeit more moderate – values could reduce w significantly.) The outflow is most marked where $|x-X|$ is small ; in other words, very near the characteristic place.

The 'source' of this multidirectional outflow is the abrupt fall of u_S to zero from a maximum value

$$u_S^{\max}(Z) \tag{139}$$

which, as here indicated, varies with Z across the width of the basilar membrane – although the maximum is reached at a position $X = X_m$ (just before the characteristic place) which is essentially independent of Z. In (138), the 'source strength' might be defined as

$$q = \frac{1}{\pi}\int_{X \text{ near } X_m}\int\left(-\frac{\partial u_S}{\partial X}\right) dX\, dZ = \frac{1}{\pi}\int u_S^{\max}(Z)\, dZ, \tag{140}$$

which, having the dimensions 'velocity times distance' is not so much a flow rate in the true sense as some 'two-dimensional analogue' of a flow rate. For x near X_m, the mean 'far field' flow pattern associated with this source of strength (140) is given by (138) and by the analogous equation for v as

$$w = \frac{q}{2}\frac{yz}{(y^2+z^2)^{\frac{3}{2}}}, \quad v = \frac{q}{2}\frac{y^2}{(y^2+z^2)^{\frac{3}{2}}}, \tag{141 a, b}$$

if the origin of z is taken as the centroid of the distribution (139).

Equation (141 a) may be thought to have some modest value as suggesting an order of magnitude for w at inner hair cells, but such a value is limited by the equation's excessive dependence on an over-simplified geometry. We learn far more by recognizing the velocity field (141) as two-dimensional and solenoidal, and as directing away from the origin into the region of fluid $y > 0$ a total flow

$$q \text{ per unit length.} \tag{142}$$

In this sense, q is truly a 'two-dimensional source strength', although (141 a, b) describe not so much an omnidirectional source as one with a certain bias against directions close to the resistive solid boundary (figure 9).

The source-like motion, then, is by no means irrotational; and we must avoid giving any impression that simple considerations from the equation of continuity associate an unbalanced inflow (139) to the characteristic place with a rate of outflow (140) per unit length. On the contrary, the momentum equation (describing

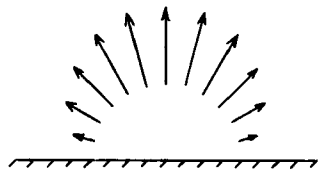

FIGURE 9. The two-dimensional and solenoidal distribution (141) of vector velocity is exhibited for points at a particular distance from the origin. While the velocity's direction is everywhere outwards from the 'source', its magnitude is relatively less in directions close to the solid boundary (hatched line).

'traction' by the streaming motion's boundary values) plays a key role in determining the value (140) of q, including especially the factor π^{-1} which appears outside the integral.

At this stage, the true geometry of the scala media can be properly allowed for if, near the characteristic place, we regard (140) as defining the mean streaming outflow per unit length from the basilar membrane (figure 9) and then take into account effects of the detailed geometry in determining what happens to that flow. If, for example, it were to be mainly channelled through the gap between inner hair cells and the tectorial membrane, then the deflecting force acting on stereocilia would be directly determined by the flow rate q per unit length through that gap. This idea, to be studied further in our concluding §10, indicates the potential importance of the above inference of an outflow rate q from a distribution u_S of effective slip velocity forced by Reynolds stresses.

In the meantime, we consider briefly whether the slip velocity's z-component w_S, estimated in §7, could make contributions to the value of w near inner hair cells comparable to those of u_S itself. Superficially, this might be considered possible because the direction of w_S coincides with the direction of those mean streaming velocities w that could deflect inner-hair-cell stereocilia. This 'advantage' is massively outweighed, however, by two considerations:

(i) the relatively smaller magnitude of w_S as estimated in (118); and

(ii) the fact that its leading term (the one independent of k) takes the form of a z-derivative

$$-\frac{\partial}{\partial z}\left(\frac{V^2}{8\omega}\right) \tag{143}$$

and therefore integrates to zero across the width of the basilar membrane.

We can briefly indicate the importance of this last point by a calculation using (as above) the simple 'half-plane' geometry ($y > 0$) for the fluid region.

Then the stresslet solution (135) related to the boundary value (136) may be rotated through 90° to yield a corresponding solution with

$$w = \frac{3z^2y}{2\pi r^5}, \quad v = \frac{3zy^2}{2\pi r^5}, \quad u = \frac{3xyz}{2\pi r^5} \quad \text{related to} \quad w_S = \delta(x)\,\delta(z). \tag{144}$$

The value of w related to a general boundary distribution $w_S(x, z)$ may then be written down as

$$w = \frac{3}{2\pi}\int_{-\infty}^{\infty}\int_{-\infty}^{\infty} w_S(X, Z)\left\{\frac{(z-Z)^2 y}{[(x-X)^2+y^2+(z-Z)^2]^{\frac{5}{2}}}\right\}\mathrm{d}X\,\mathrm{d}Z; \tag{145}$$

but a comparison with (137) quickly shows (145) to be much the smaller if w_S is dominated by the z-derivative term (143) which integrates to zero. Then, indeed, an integration by parts shows the far-field behaviour of (145) to be dominated by the Z-derivative of the term in curly brackets. Therefore, it exhibits inverse-cube decay, in stark contrast to the much slower inverse-first-power decay obtained above for the contribution from u_S; and it need not be further considered.

We may similarly conclude that little account need be taken of the differences (§5) between the Euler and Lagrange mean flows at the locations of inner hair cells, because those differences fall away exponentially with distance from the basilar membrane, the decay taking, for example, the form (68) just outside the Stokes layer. Fortunately, then, we are not compelled to probe exhaustively the difficult question of whether the mean deflecting force will be more responsive to the Euler or to the Lagrange mean flow; very briefly, however, we note that the answer must be strongly influenced by whether responses of stereocilia to vibrations at the characteristic frequency are stiffness-dominated or inertia-dominated. Stereocilia may, perhaps, predominantly 'feel' the Euler mean motion (mean velocity at a fixed point) in the former case and the Lagrange mean motion (mean velocity following a fluid particle) in the latter.

10. Fluid-mechanical conclusions

This is not a paper which seeks to draw any biological conclusions. It does, on the other hand, attempt a comprehensive review of those mean streaming motions that may be generated by cochlear travelling waves; and the fluid-mechanical conclusions of this review can now (perhaps) be summarized, with cross-references to parts of the paper where each is substantiated.

For acoustic components of a particular frequency ω, a fairly steep increase in wave amplitude to its maximum at the characteristic place is immediately followed by a precipitous fall to zero, as illustrated in figure 1 and interpreted in §2 generally. The three-dimensional distribution of wave energy has been described (§3) and shown, very near the characteristic place, to involve locally two-dimensional motions close to each point of the basilar membrane (§4). Here, local mean streaming motions (§§5–8) are generated through the action of mean momentum flow (Reynolds stress) in producing an effective slip velocity.

This slip velocity, given by the classical acoustic-streaming formula (92) at moderate wavenumbers and by the modified formula (121) at high wavenumbers, displays once again a fairly steep increase to a maximum (139) at the characteristic place, followed by an extremely precipitous decrease, which in turn (§9) creates in the local cochlear cross-section a mean outflow (140) per unit length from the basilar membrane (figure 9). If the cross-sectional geometry acts to channel such a flow through the space between inner hair cells and the tectorial membrane, then the stereocilia of those cells may be deflected by this mean throughflow.

In order to make the above suggestions quantitative, we must use (140) to estimate the outflow q per unit length emerging from the basilar membrane at the characteristic place. The estimation needs to be attempted both for waves that are freely propagated and attenuated (§2) and for waves experiencing additional amplification as a result of forcing movements by outer hair cells.

Unfortunately, however, our analysis of the latter process (§3) remains too incomplete to permit useful estimates to be attempted. This is particularly to be regretted since the amplified waves can be expected to generate enhanced mean

streaming motions. It means that, in considering free waves below, we must continually recall that our estimates of streaming may be underestimates when forcing is present.

Waves that are freely propagated, and attenuated at a proportional rate D, have the above-noted 'fairly steep increase, followed by a precipitous fall' of their energy E per unit length of cochlea described either (i) by (18) for E in integral form or (ii) by the equivalent differential equation (19). Each of these equations shows us readily that E takes its maximum value at the position x where the condition

$$\mathrm{d}U/\mathrm{d}x = -D \tag{146}$$

is satisfied. Beyond that maximum, where the integral in (18) grows without any limit, its negative exponential plummets to zero.

The place x where the energy E per unit length is a maximum must also be a place of peak velocity amplitude V (at each location z across the width of the basilar membrane). On the other hand, the slip velocity u_S has not yet reached its maximum velocity (139) at such a place. In the classical acoustic-streaming formula (92), for example, the V^2 factor in the first term has reached its maximum but the k factor is still increasing with x. The second term, furthermore, begins to make a positive contribution to u_S where V is decreasing beyond its maximum. Thus the value of the first term where V is greatest is certainly an underestimate of $u_S^{\max}$ itself; and the same conclusion follows from the modified formula (121) because the extra factor σ grows from 1 to 2 at very high wavenumber.

In a strictly preliminary estimate of $u_S^{\max}$, however, we can use, at the place where condition (146) is satisfied, just the first term

$$u_S = \tfrac{1}{4} V^2 k\omega^{-1} \tag{147}$$

in (92), knowing it to be a distinctly 'conservative estimate' (more precisely, an underestimate) because, alongside its disregard of any forcing (see above), it neglects (a) the continuing increase in k; (b) the extra factor $\sigma > 1$ in the more accurate equation (121); and (c) the positive contribution, where V is decreasing, from the second term in (92) – or, in (121), from the second term up to where τ changes sign. For the moment, we postpone application of considerations (a), (b) and (c), and utilize (147) as our first conservative estimate for $u_S^{\max}$.

Its use, by (140), gives an equation

$$q = \frac{1}{4\pi} k\omega^{-1} \int V^2 \,\mathrm{d}z \tag{148}$$

for the mean outflow per unit length from the basilar membrane at the characteristic place. Here, the value of $k\omega^{-1}$ (the reciprocal phase velocity) may be estimated from (146) which must be satisfied where V is a maximum. With expression (13) for U it takes the form

$$\frac{s'(x)\,[s(x)-s(x_r)]\,[s(x)+s(x_r)]}{2A\rho\omega[s(x)]^2} = -D, \tag{149}$$

so that (11) for k gives

$$k\omega^{-1} = \frac{1}{D}\left[-\frac{s'(x)}{s(x)}\frac{s(x)+s(x_r)}{2s(x)}\right] \doteqdot \frac{1}{DL}. \tag{150}$$

In (150), the term in square brackets is taken, to a close approximation near $x = x_r$, as the downward gradient of $\ln [s(x)]$ along the cochlea; which may be represented as a constant L^{-1} (where L signifies the e-folding distance for basilar-membrane stiffness), and estimated as the overall decrease in $\ln [s(x)]$ along the cochlea's length, divided by that length.

A similar estimate for the proportional dissipation rate D must be based on its definition which makes DE the rate of energy dissipation per unit length of cochlea. But the energy dissipation rate Δ per unit area is given by (66) for each of the two boundary layers attached to the basilar membrane, from which it follows that the overall rate per unit length is

$$DE = \rho(\tfrac{1}{2}\omega\nu)^{\frac{1}{2}} \int V^2 \, \mathrm{d}z. \tag{151}$$

The combined equations (148), (150) and (151) now give

$$q \doteq \frac{E^{\max}}{4\pi\rho(\tfrac{1}{2}\omega\nu)^{\frac{1}{2}} L} \tag{152}$$

as our preliminary 'conservative' estimate for the mean outflow q per unit length. Here, L is the e-folding distance for basilar-membrane stiffness (as above) while E has been written as $E^{\max}$ because our calculation is concentrated on the place where the condition (146) holds so that the wave energy E per unit length takes its maximum value.

This simple first estimate (152) is now relatively easy to improve in two stages. First, we take into account considerations (*a*), (*b*) and (*c*) above while continuing to use the moderate-wavenumber formulae (92) for u_S and (66) for Δ. This yields a value of q increased by a factor approaching 1.5, resulting from values of u_S that rise (figure 10) to a maximum almost 50% greater than at the place where $E = E^{\max}$. At that maximum the value of k is increased, but again only by a moderate factor around 1.5; and the analysis is completed by showing that the non-dimensional wavenumber κ then remains sufficiently small for the numerical results to be affected to only a modest extent.

The curves in figure 10 are obtained from the distribution (18) of E for values of x between x_m (the value where $E = E^{\max}$) and x_r (where E has plummeted to zero). This is an interval where, for simplicity, we can represent (130 as a quadratic variation

$$U = \tfrac{1}{2}\eta(x_r - x)^2 \tag{153}$$

of the group velocity U with x; here, (146) defining x_m makes

$$\eta(x_r - x_m) = D. \tag{154}$$

Therefore, (18) gives

$$\begin{aligned} \frac{E}{E^{\max}} &= \frac{(x_r - x_m)^2}{(x_r - x)^2} \exp\left(-\int_{x_m}^{x} \frac{2(x_r - x_m)}{(x_r - x)^2} \mathrm{d}x \right) \\ &= \frac{(x_r - x_m)^2}{(x_r - x)^2} \exp\left(-2\frac{x - x_m}{x_r - x} \right). \end{aligned} \tag{155}$$

Similarly, we can represent (11) as a linear variation

$$k^{-1} = \beta(x_r - x) \tag{156}$$

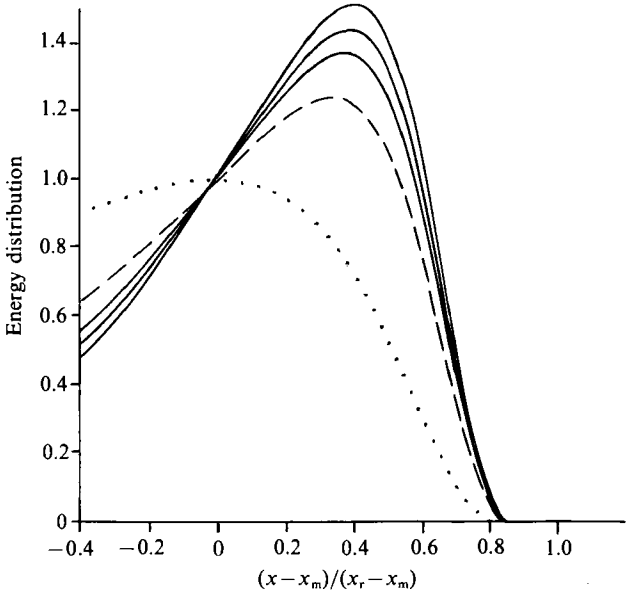

FIGURE 10. The energy distribution (155) is shown (dotted line), while the modifying factor (159) is plotted (solid lines) for three positive values (0.1, 0.15 and 0.2) of β and also (broken line) for $\beta = 0$.

of k^{-1} with x, where

$$\beta = -s'(x_r)/(A\rho\omega^2) \tag{157}$$

is the value of the small parameter (14) at $x = x_r$.

Now the classical acoustic-streaming formula (92) for u_S can be written

$$\left[k - \frac{3}{2}\frac{d}{dx}\right]\tfrac{1}{4}V^2\omega^{-1}, \tag{158}$$

so that its ratio to the value of u_S where $x = x_m$ (and $dV/dx = 0$) would be

$$\left[k - \frac{3}{2}\frac{d}{dx}\right]\frac{E}{k_m E^{max}} = \frac{k}{k_m}\frac{E}{E^{max}}\left[1 - \tfrac{3}{2}k^{-1}\frac{d\ln E}{dx}\right]$$

$$= \frac{(x_r - x_m)^3}{(x_r - x)^3}\left[1 + 3\beta\frac{x - x_m}{x_r - x}\right]\exp\left(-2\frac{x - x_m}{x_r - x}\right). \tag{159}$$

This modifying factor is plotted in figure 10 for $x_m < x < x_r$ with three different values of the small parameter β. The conclusions are not very sensitive to the value of β; tentatively, we use the intermediate value $\beta = 0.15$ which represents the value (14) of $k^{-2}\partial k/\partial x$ for the cochlear travelling waves illustrated in figure 1.

On this basis, the maximum u_S^{max} for each z is increased by a factor of 1.44 over its value at $x = x_m$, so that expression (140) for q is increased to 1.44 times the preliminary estimate (152). The modifying factor would, on the other hand, be reduced to 1.24 if β were zero (broken line).

Probably, the true figure lies somewhere between these limits, because in the high-wavenumber result (121) the coefficient $\tau(\kappa)$ shows an early decrease from unity towards zero in the range $0 < \kappa < 0.1$, a range in which, by contrast, both $\sigma(\kappa)$ and

the factor (figure 12) that modifies the dissipation rate Δ remain close to unity. Then β must be replaced by $\beta\tau$ in the high-wavenumber modification of (159), and this reduction gives it a maximum value lying somewhere between 1.24 and 1.44. Such a modifying factor, applied to $u_S(z)$ for each z and thus to (152) for q, brings it numerically to

$$q = \frac{0.15E^{\max}}{\rho(\omega\nu)^{\frac{1}{2}}L}, \tag{160}$$

where the coefficient 0.15, as quoted to two significant figures, stands for a number between 0.14 and 0.16.

Such a level of uncertainty reflects a real difficulty in estimating the non-dimensional wavenumber (67). At the point x_m for maximum wave energy, the wavenumber k_m is given by (150), while D satisfies (151), so that the value of κ is

$$\kappa_m = k_m(\nu/\omega)^{\frac{1}{2}} = \frac{1}{L\sqrt{2}}\left\{\frac{E}{\int\frac{1}{2}\rho V^2\,dz}\right\}. \tag{161}$$

If basilar-membrane stiffness $s(x)$ decreases by between 3 and 4 orders of magnitude along the length of the cochlea, then $\ln[s(x)]$ decreases by between 7 and 9 so that L is between one-seventh and one-ninth of the cochlea's length (making $L\sqrt{2}$ around 6 to 7 mm in a human cochlea, for example). The factor in curly brackets, on the other hand, represents the mean distance of penetration of kinetic energy – both solid and fluid, constituting the whole of E at phases of oscillation where the basilar-membrane velocity takes its peak value V – into the cochlea. The mean penetration on both sides of the basilar membrane is likely to be less than one-fifth of the cochlear diameter (for example, less than 0.3 mm in a human cochlea) which suggests a value of (161) for κ_m not exceeding 0.05. Accordingly, even allowing for the fact that the curves in figure 10 have maxima at points where k is around $1.5k_m$, we can justifiably make the assumption $0 < \kappa < 0.1$ that was used to obtain (160).

Our definitive conclusion on the magnitude of the mean streaming outflow, q per unit length from the basilar membrane at the characteristic place, is expressed, then, by (160). For each frequency ω, this depends on quantities ρ and ν whose values for the cochlear fluids are the same as for water, on an e-folding distance L for basilar-membrane stiffness which (see above) is readily estimated, and on the maximum wave energy per unit length, $E^{\max}$. As noted earlier, however, any use of this conclusion to investigate the possibility or otherwise of a resulting mean force on stereocilia playing a part in the process of transduction by inner hair cells is postponed to a later paper.

It is a pleasure to express my warm thanks to Professor David Kemp for valuable discussions, to Dr M. E. McIntyre and Professor N. Riley for helpful comments on a first draft of the paper, and to the Leverhulme Trust for generous support.

Appendix A. High-wavenumber modifications to the viscous dissipation rate

A.1. *Introduction*

In this Appendix we investigate how the rate of energy dissipation due to viscous action in fluid near the basilar membrane may be modified at *high wavenumbers*, comparable with the reciprocal of the Stokes boundary-layer thickness. The

calculation is facilitated by the fact that such wavenumbers are large enough for the motions to be locally two-dimensional.

There are classical reasons for expecting the calculated dissipation to be greater than the simple rate of dissipation in a Stokes boundary layer. For example, the two-dimensional motions occurring when progressive water waves propagate in a flat-bottomed channel suffer dissipation equal to the sum of the dissipation in the Stokes layer on the bottom and the rate of viscous dissipation for the irrotational flow external to the boundary layer (Lighthill 1978*b*, §3.5).

Against this background it may be seen as interesting that, in the analogous case when the free surface is replaced by a solid (though compliant) basilar membrane, we do once more find an increase – and yet by a lot less than would be obtained if we simply added the dissipation rates in the Stokes layer and in the external irrotational flow.

Dissipation rate is, indeed, specified by a quadratic expression so that it can include 'cross-terms' between the distributions of shear in the Stokes layer and in the external irrotational flow. These shears are found to be correlated negatively; accordingly, the cross-terms contribute negatively to the total dissipation rate. This, in consequence, is increased by substantially less than we would have been led to expect by the classical calculation (in which no such negative correlation occurs); and a similar trend is found to be continued even at wavenumbers so high that, effectively, no irrotational-flow region is present.

A.2. *Equations for the dissipation rate*

The linearized momentum and continuity equations

$$\rho i\omega \boldsymbol{u} = -\nabla p + \mu \nabla^2 \boldsymbol{u}, \quad \nabla \cdot \boldsymbol{u} = 0 \tag{A 1}$$

for motions of an incompressible fluid (of density ρ and viscosity μ) at radian frequency ω yield the following separate equations for the pressure p and velocity $\boldsymbol{u}$:

$$\nabla^2 p = 0, \quad \nabla^2(\nabla^2 - i\omega\nu^{-1})\boldsymbol{u} = 0 \tag{A 2}$$

where $\nu = \mu/\rho$ is the kinematic viscosity. Two-dimensional solutions $\boldsymbol{u} = (u, v)$ of (A 2) for $y \geqslant 0$ which satisfy

$$u = 0, \quad v = V e^{i(\omega t - kx)} \quad \text{on} \quad y = 0 \tag{A 3}$$

(corresponding to lateral oscillatory motions of the basilar membrane with velocity amplitude V) take the form

$$u = iA\, e^{i(\omega t - kx)}(e^{-ky} - e^{-Ky}), \quad v = A\, e^{i(\omega t - kx)}(e^{-ky} - kK^{-1} e^{-Ky}), \tag{A 4}$$

where the constants A and K satisfy the equations

$$A(1 - kK^{-1}) = V, \quad K^2 = k^2 + i\omega\nu^{-1}. \tag{A 5}$$

The general character of these solutions depends on the value of a non-dimensional wavenumber

$$\kappa = k(\nu/\omega)^{\frac{1}{2}}. \tag{A 6}$$

It is for small κ that K far exceeds k in absolute value; then the motion is effectively divided into (i) an external irrotational flow and (ii) a Stokes-layer flow, given respectively by the first and the second terms in each of equations (A 4).

The mean dissipation rate per unit volume may be written

$$2\mu \langle (\partial u/\partial x)^2 + (\partial v/\partial y)^2 \rangle + \mu \langle (\partial u/\partial y + \partial v/\partial x)^2 \rangle \tag{A 7}$$

which, with u and v given by (naturally) the real parts of (A 4), becomes

$$2\mu\,|A|^2k^2\{|\mathrm{e}^{-ky}-\mathrm{e}^{-Ky}|^2+|\mathrm{e}^{-ky}-\tfrac{1}{2}(k^{-1}K+kK^{-1})\,\mathrm{e}^{-Ky}|^2\} \tag{A 8}$$

with the two separate terms in (A 7) represented, respectively, by the two terms in (A 8). From this quadratic expression it is already clear that the positive contributions to dissipation proportional to e^{-2ky} and $|\mathrm{e}^{-2Ky}|$ will be offset by a negative contribution from the 'cross-terms' related to $\mathrm{e}^{-(k+K)y}$.

With terms of the three different kinds collected together, (A 8) becomes

$$2\mu\,|A|^2k^2\{2\mathrm{e}^{-2ky}-\mathrm{Re}\,[(2+k^{-1}K+kK^{-1})\,\mathrm{e}^{-(k+K)y}]+(1+\tfrac{1}{4}|k^{-1}K+kK^{-1}|^2)\,|\mathrm{e}^{-2Ky}|\}, \tag{A 9}$$

with the negative cross-terms appearing in the middle. An integration of (A 9) from $y=0$ to $y=\infty$ gives the total dissipation rate Δ per unit area of solid surface as

$$2\mu\,|A|^2k^2\{k^{-1}-\mathrm{Re}\,(k^{-1}+K^{-1})+(1+\tfrac{1}{4}|k^{-1}K+kK^{-1}|^2)\,(2\,\mathrm{Re}\,K)^{-1}\}, \tag{A 10}$$

where the substantial negative contribution from cross-terms is made particularly clear.

Finally, (A 10) may be written

$$\tfrac{1}{4}\mu\,|A|^2\,|K|^{-2}(\mathrm{Re}\,K)^{-1}[-8k^2(\mathrm{Re}\,K)^2+4k^2\,|K|^2+|K^2+k^2|^2], \tag{A 11}$$

which can be simplified, since (A 5) for K^2 gives

$$k^2=\mathrm{Re}\,(K^2)=2(\mathrm{Re}\,K)^2-|K|^2,\quad |K^2+k^2|^2=4k^4+\omega^2\nu^{-2}, \tag{A 12}$$

to the form

$$\tfrac{1}{4}\mu\,|A|^2|K|^{-2}(\mathrm{Re}\,K)^{-1}\omega^2\nu^{-2}. \tag{A 13}$$

In terms of the velocity amplitude V given by (A 5), the energy dissipation rate per unit area (A 13) becomes

$$\Delta=\tfrac{1}{4}\mu V^2\,|K-k|^{-2}(\mathrm{Re}\,K)^{-1}\,|K^2-k^2|^2=\tfrac{1}{4}\mu V^2(\mathrm{Re}\,K)^{-1}\,|K+k|^2. \tag{A 14}$$

A.3. *Discussion of the results*

In a high-wavenumber limit, specified by (A 6) and (A 5) as one with κ large so that K is close to k, the dissipation rate (A 14) becomes $\Delta=\mu kV^2$. For general wavenumbers, we may write the ratio $\Delta/\mu kV^2$ as a function of κ in the form

$$\frac{\Delta}{\mu kV^2}=\frac{(\kappa^4+1)^{\frac{1}{2}}+\kappa^2}{4\kappa\,\mathrm{Re}\,(\kappa^2+\mathrm{i})^{\frac{1}{2}}}+\tfrac{1}{2}, \tag{A 15}$$

where the additional $\frac{1}{2}$ appears because the square $|K+k|^2$ in (A 14) includes a cross term $2k\,\mathrm{Re}\,K$.

Equation (A 15) is particularly interesting for quite small κ. Then the first term is close to the value $(2\kappa\sqrt{2})^{-1}$ corresponding to dissipation in the Stokes boundary layer, whereas the second term is only one-quarter of the rate of dissipation as classically calculated for the external irrotational flow on its own. As already explained, it is the negative correlation between those shearing motions in the two fields which combine into the dissipation rate (A 8) per unit volume that makes the integrated rate Δ substantially smaller than would be derived by simply adding up the two contributions.

It is noteworthy also that the limiting value 1 of (A 15) as κ becomes large represents only one-half of the dissipation for an irrotational flow compatible with the boundary condition on v alone. Evidently, this is because the motion in this limit

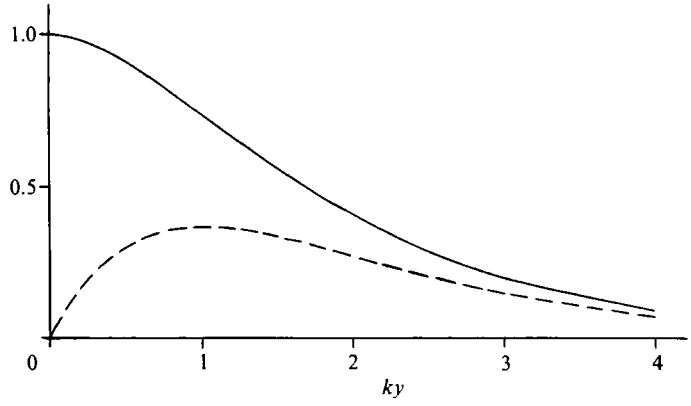

FIGURE 11. Illustrating the limiting forms (119) for extremely high wavenumber of the amplitude of oscillation of the y-velocity (solid line, representing v/V) and the x-velocity (broken line, representing $|u|/V$) as functions of ky.

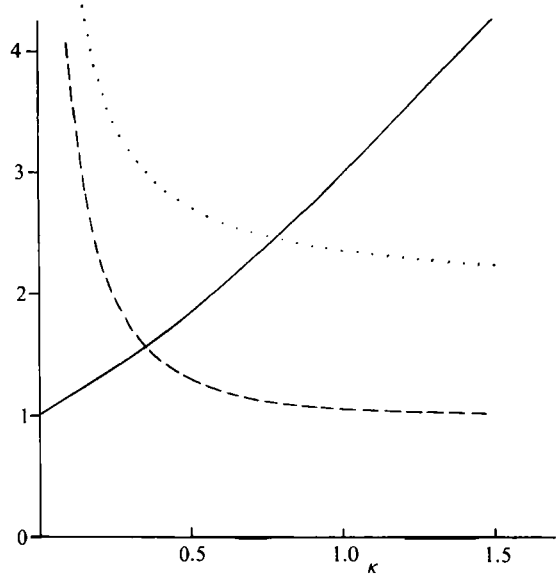

FIGURE 12. Plotting high-wavenumber modifications to the rate, Δ per unit area of basilar membrane, of energy dissipation within the motion on either side of it. The ratio (A 15) is shown as the broken line, here contrasted with the dotted-line values that would be obtained by (erroneously) adding the dissipations in the Stokes-layer and irrotational-flow fields. The ratio (A 16) of Δ to its value (66) on the Stokes-layer approximation is shown as a solid line.

has become far from irrotational, with values of u substantially reduced relative to those of v (see figure 11; actually, (A 4) imply that $|u|$ takes a maximum value of about Ve^{-1}, compared with a maximum of V in irrotational flow).

The broken line in figure 12 shows expression (A 15) *quâ* function of κ as close to the Stokes-layer value $(2\kappa\sqrt{2})^{-1}$ for $\kappa < 0.1$ and as close to its asymptotic value 1 for $\kappa > 1$. The figure contrasts this accurately calculated result with the bigger (dotted-line) value $(2\kappa\sqrt{2})^{-1}+2$ which would be obtained by (erroneously) adding the dissipations in the Stokes-layer and irrotational flow fields.

Lastly, the solid line in figure 12 represents the ratio of (A 15) to its simple Stokes-layer limit $(2\kappa\sqrt{2})^{-1}$. Thus, the quantity plotted is the ratio

$$\Delta/[\rho V^2(\tfrac{1}{8}\omega\nu)^{\frac{1}{2}}] \tag{A 16}$$

of Δ to the value (66) calculated on the Stokes-boundary-layer approximation.

This plain-line enhancement factor is seen to be quite substantial (even though smaller than might have been foreseen from an erroneous argument) and it reconfirms the steep decay of wave energy as the wavenumber becomes large. This is important in the context of the present paper because the associated decay in wave momentum becomes available to generate streaming motions.

Appendix B. High-wavenumber modifications to shear-stress streaming

B.1. *Introduction*

In this Appendix we make further use of the locally two-dimensional solutions derived in Appendix A for wavenumbers comparable to the reciprocal of the Stokes-boundary-layer thickness. The Reynolds shear stress

$$\rho\langle uv\rangle \tag{B 1}$$

is calculated, and used to determine the associated mean motions which we designate as shear-stress streaming.

There are, of course, two alternative definitions of mean motion: the Euler mean

$$\boldsymbol{u}_{\mathrm{E}} \tag{B 2}$$

or average motion at a fixed point in space, and the Lagrange mean

$$\boldsymbol{u}_{\mathrm{L}} \tag{B 3}$$

or average motion for a given particle of fluid. The difference between them is defined as

$$\boldsymbol{u}_{\mathrm{M}} = \boldsymbol{u}_{\mathrm{L}} - \boldsymbol{u}_{\mathrm{E}}. \tag{B 4}$$

Its x-component u_{M} is calculated for the velocity field (A 4) in §B.2 (the corresponding v_{M} is found to be zero) as assuming positive values for larger y and negative values for smaller y in such a way that the net mass transport

$$\int_0^\infty u_{\mathrm{M}}\,\mathrm{d}y \tag{B 5}$$

is zero. This conclusion, furthermore, is found to hold even when k is complex so that equations (A 4) are describing a spatially growing or decaying velocity field.

The other importance of $\boldsymbol{u}_{\mathrm{M}}$ lies in the boundary condition that it imposes on u_{E} at the solid surface. The fact that particles at the solid surface cannot move tangentially implies that u_{L} is zero there. It follows that the boundary condition on u_{E} takes the form

$$(u_{\mathrm{E}})_{y=0} = -(u_{\mathrm{M}})_{y=0}. \tag{B 6}$$

In §B.3 we use this boundary condition to determine the Euler mean motion u_{E} near the wall from a balance

$$\rho\langle uv\rangle = \mu\partial u_{\mathrm{E}}/\partial y \tag{B 7}$$

between the Reynolds shear stress (B 1) and the viscous shear stress $\mu\partial u_{\mathrm{E}}/\partial y$ which

dominates the Euler-flow stress field in the thin layer where $\langle uv \rangle$ takes values significantly different from zero. This leads to a determination of the shear-stress streaming u_S, defined as the value

$$u_S = -(u_M)_{y=0} + \nu^{-1} \int_0^\infty \langle uv \rangle \, dy \tag{B 8}$$

of the solution u_E to (B 7) and (B 6) at the edge of this thin layer.

The calculations in §B.3 for real k (waves without spatial growth or decay) give a value of u_S in the form

$$u_S = \tfrac{1}{4} V^2 k \omega^{-1} \sigma \, (\kappa) \tag{B 9}$$

where κ is the non-dimensional parameter (A 6) and for small κ the function $\sigma(\kappa)$ is close to 1 so that (B 9) agrees with the Stokes-layer calculation. As κ increases, however, the function $\sigma(K)$ grows slowly, to reach an asymptote of 2 for large κ.

Finally, calculations in §B.4 with k given a small imaginary part allow us to derive the additional shear-stress streaming associated with spatial growth or decay of the velocity amplitude V. Equation (B 8) is then modified to

$$u_S = \tfrac{1}{4} V^2 k \omega^{-1} \sigma(\kappa) - \tfrac{1}{4} V (dV/dx) \, \omega^{-1} \tau_1(\kappa) \tag{B 10}$$

where $\tau_1(\kappa)$ like $\sigma(\kappa)$ is close to 1 for small κ (so that B 10) agrees with the Stokes-layer calculation); however, $\tau_1(\kappa)$ is found to decrease at first as κ increases, and then to take negative values before it finally rises to its asymptote of zero for large κ.

B.2. *The mean motion $\boldsymbol{u}_M$ and its zero net mass flow*

In the velocity field (A 4), a particle's first-order displacements $(\delta x, \delta y)$ take the form

$$\delta x = u/(i\omega), \quad \delta y = v/(i\omega) \tag{B 11}$$

and its mean velocity u_M is

$$u_M = \langle (\partial u/\partial x) \, \delta x + (\partial u/\partial y) \, \delta y \rangle. \tag{B 12}$$

We calculate this mean using the rule that the average value of the product of two quantities specified as the real parts of complex multiples of $e^{i\omega t}$ is half the real part of a product of one quantity with the complex conjugate of the other. Thus

$$\begin{aligned} u_M = \tfrac{1}{2} \operatorname{Re} [&(A/\omega) (e^{-ky} - e^{-Ky}) \bar{A} \bar{k} (e^{-\bar{k}y} - e^{-\bar{K}y}) \\ &+ iA (-k e^{-ky} + K e^{-Ky}) \bar{A} (-i\omega)^{-1} (e^{-\bar{k}y} - \bar{k}\bar{K}^{-1} e^{-\bar{K}y})], \end{aligned} \tag{B 13}$$

where the δx in (B 12) has been placed before the $\partial u/\partial x$ but the δy after the $\partial u/\partial y$.

Equation (B 13) for the mean motion u_M may be simplified in various ways, but for the analysis in this paper such simplification is unnecessary. We require only the boundary value

$$(u_M)_{y=0} = -\tfrac{1}{2} |A|^2 \omega^{-1} |1 - kK^{-1}|^2 \operatorname{Re} K = -\tfrac{1}{2} V^2 \omega^{-1} \operatorname{Re} K, \tag{B 14}$$

derived from the second line of (B 13) (since the first vanishes for $y = 0$) in two alternative forms which (A 5) shows to be equivalent; and we need the mass-flow integral

$$\begin{aligned} \int_0^\infty u_M \, dy = \tfrac{1}{2} |A|^2 \omega^{-1} \operatorname{Re} \int_0^\infty [&\bar{k} e^{-(k+\bar{k})y} - \bar{k} e^{-(k+\bar{K})y} - \bar{k} e^{-(\bar{k}+K)y} \\ &+ \bar{k} e^{-(K+\bar{K})y} + k e^{-(k+\bar{k})y} - k\bar{k}\bar{K}^{-1} e^{-(k+\bar{K})y} - K e^{-(\bar{k}+K)y} + \bar{k}K\bar{K}^{-1} e^{-(K+\bar{K})y}] \, dy \end{aligned} \tag{B 15}$$

in which the terms involving the four different negative exponentials may be lumped together and integrated to give

$$\int_0^\infty u_{\mathrm{M}}\,\mathrm{d}y = \tfrac{1}{2}|A|^2\omega^{-1}\,\mathrm{Re}\left[\frac{k+\bar{k}}{k+\bar{k}} - \bar{k}\frac{1+k\bar{K}^{-1}}{k+\bar{K}} - \frac{\bar{k}+K}{\bar{k}+K} + k\frac{1+K\bar{K}^{-1}}{K+\bar{K}}\right]$$
$$= \tfrac{1}{2}|A|^2\omega^{-1}\,\mathrm{Re}\,[1-\bar{k}\bar{K}^{-1}-1+k\bar{K}^{-1}] = 0. \tag{B 16}$$

It is remarkable that the mean motion u_{M} has zero net mass flow even when the wavenumber k is allowed to have a complex value, corresponding to waves with spatial growth or decay. For some further discussion of this result, see §5.

We may note also that a calculation similar to that in (B 13) gives

$$v_{\mathrm{M}} = \langle(\partial v/\partial x)\,\delta x + (\partial v/\partial y)\,\delta y\rangle = 0 \quad \text{everywhere} \tag{B 17}$$

so that (B 13) specifies the entire mean motion $\boldsymbol{u}_{\mathrm{M}}$ as a flow in the negative x-direction for small y balanced by an equal flow in the positive x-direction for larger values of y. Essentially, (B 17) is derived from the fact that the equation of continuity makes $\partial v/\partial y = \mathrm{i}ku$, which with $\partial v/\partial x = -\mathrm{i}kv$ and (B 11) for δx and δy gives $v_{\mathrm{M}} = 0$.

B.3. *Shear-stress streaming for waves of uniform amplitude*

The expression (B 8) for shear-stress streaming can be written, using the rule for mean values quoted in §B.2, as

$$u_{\mathrm{S}} = -(u_{\mathrm{M}})_{y=0} + \nu^{-1}\int_0^\infty \tfrac{1}{2}\,\mathrm{Re}\,[-\mathrm{i}\bar{A}(\mathrm{e}^{-\bar{k}y}-\mathrm{e}^{-\bar{K}y})A(\mathrm{e}^{-ky}-kK^{-1}\mathrm{e}^{-Ky})]\,\mathrm{d}y$$
$$= \tfrac{1}{2}V^2\omega^{-1}\,\mathrm{Re}\,K + \tfrac{1}{2}\nu^{-1}|A|^2\,\mathrm{Re}\left[\mathrm{i}\left(\frac{1}{k+\bar{K}} + \frac{k}{K(\bar{k}+K)} - \frac{k}{K(K+\bar{K})}\right)\right], \tag{B 18}$$

which includes terms from just three of the cross-products of exponentials in the integral because the fourth is purely real. We calculate (B 18) in this section for real k (so that $\bar{k} = k$, corresponding to waves of uniform amplitude) before investigating cases with spatial growth or decay in §B.4.

Then (B 18), with its first term represented by the second of the two forms (B 14), and with A substituted from (A 5), becomes

$$u_{\mathrm{S}} = \tfrac{1}{2}V^2\omega^{-1}\,\mathrm{Re}\,K + \tfrac{1}{2}\nu^{-1}\frac{|K|^2V^2}{|K-k|^2}\,\mathrm{Re}\left[\mathrm{i}\frac{|K|^2(k+K)+k\bar{K}(k+\bar{K})}{|K|^2\,|K+k|^2} - \mathrm{i}\frac{k\bar{K}}{2|K|^2\,\mathrm{Re}\,K}\right] \tag{B 19}$$

which can be simplified, using the consequences

$$|K^2-k^2|^2 = \omega^2\nu^{-2}, \quad 2\,\mathrm{Re}\,K\,\mathrm{Im}\,K = \omega\nu^{-1} \tag{B 20}$$

of the definition (A 5), as

$$u_{\mathrm{S}} = \tfrac{1}{2}V^2\nu\omega^{-2}\Big[2(\mathrm{Re}\,K)^2\,\mathrm{Im}\,K - |K|^2\,\mathrm{Im}\,K + k^2\,\mathrm{Im}\,K + 2k\,\mathrm{Re}\,K\,\mathrm{Im}\,K$$
$$- \frac{k\,\mathrm{Im}\,K\,|K+k|^2}{2\,\mathrm{Re}\,K}\Big]. \tag{B 21}$$

However, because of two further consequences

$$(\mathrm{Re}\,K)^2-(\mathrm{Im}\,K)^2 = k^2, \quad |K+k|^2 = |K|^2+2k\,\mathrm{Re}\,K+k^2 = 2(k+\mathrm{Re}\,K)\,\mathrm{Re}\,K \tag{B 22}$$

of the definition (A 5), the first two terms within the square brackets are equal to the

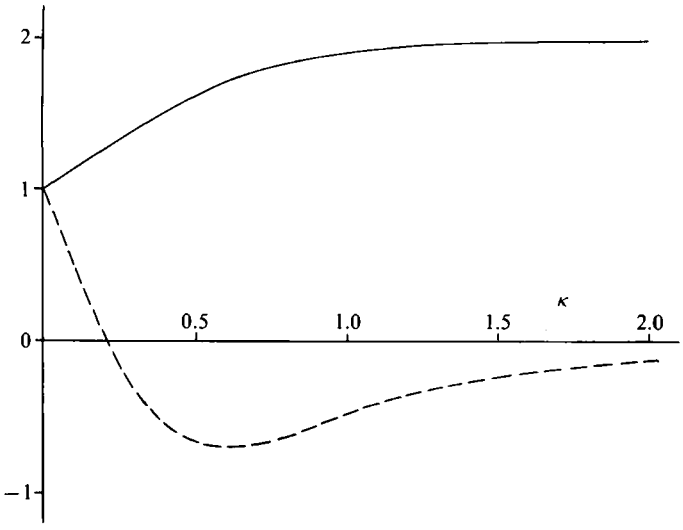

FIGURE 13. Plotting high-wavenumber modifications to shear-stress streaming. The solid line gives the factor $\sigma(\kappa)$ in (B 9) by which shear-stress streaming for uniform-amplitude waves is altered, while the broken line gives the coefficient $\tau_1(\kappa)$ in (B 29) that modifies additional shear-stress streaming due to wave growth or decay.

third while the last one (occurring with negative sign) is one-half of all the others put together. Finally, then, with $\mathrm{Im}\, K$ eliminated by use of the second of equations (B 20), we infer that

$$u_S = \tfrac{1}{4}V^2 k\omega^{-1}[1 + k(\mathrm{Re}\, K)^{-1}]: \tag{B 23}$$

a satisfactorily simple expression which coincides with the Stokes-layer result for small κ (when $\mathrm{Re}\, K$ is much greater than k) but rises to twice as much in the high-wavenumber limit (κ large) when K becomes closely equal to k. This last is a limit in which $\langle uv \rangle$ vanishes and the value of u_S is dominated by the first term in expression (B 18), derived simply from the boundary condition (B 6).

Figure 13 shows the form of the non-dimensional quantity $\sigma(\kappa)$ defined by (B 9) as the factor by which the Stokes-layer result has to be modified at higher wavenumbers. We see from (B 23) that

$$\sigma(\kappa) = 1 + \kappa[\mathrm{Re}\, (\kappa^2 + \mathrm{i})^{\frac{1}{2}}]^{-1} \tag{B 24}$$

and from figure 13 that $\sigma(\kappa)$ is close to its Stokes-layer value 1 for $\kappa < 0.1$ and to its high-wavenumber asymptotic value 2 for $\kappa > 1$.

B.4. *Additional shear-stress streaming due to wave growth or decay*

The biggest streaming effect associated with the spatial growth or decay of waves is the normal-stress streaming to be calculated in Appendix C. This is a streaming motion near the solid boundary generated by that spatial gradient in normal Reynolds stresses which, of course, may accompany any spatial gradient in wave amplitude.

However, wave growth or decay does also produce some additional shear-stress streaming. Physically, this is because gradients of the velocity's x-component u in the x-direction generate (through the equation of continuity) additional terms in the velocity's y-component v which can contribute to the Reynolds shear stress (B 1) and so also to the shear-stress streaming (B 8). In a simple Stokes boundary layer, this augments by 50% the normal-stress streaming.

Here we calculate the corresponding effect at higher wavenumbers, finding once more that the additional shear-stress streaming follows a trend similar to that of the normal-stress streaming (derived in Appendix C) and produces some numerical augmentation thereof. However, both of them tend to zero for very large wavenumbers (unlike the main shear-stress streaming in §B.3) after first changing sign.

We are looking, then, for a correction to the normal-stress streaming which, like it, takes the form of a constant multiple of $V\mathrm{d}V/\mathrm{d}x$, in terms of that spatial gradient $\mathrm{d}V/\mathrm{d}x$ of velocity amplitude which characterizes wave growth or decay. Such a correction can be obtained from the general expression (B 18) for shear-stress streaming, with k complex, by working out its first-order change when a real value of k is replaced by $k+\mathrm{i}\epsilon$ with ϵ small. Then the resulting additional term in the form of a multiple of $V^2\epsilon$ (with ϵ, as (A 4) and (A 5) imply, representing $V^{-1}\mathrm{d}V/\mathrm{d}x$) must signify an additional shear-stress streaming equal to the same multiple of $V\mathrm{d}V/\mathrm{d}x$.

This programme faces us with the problem of calculating the first-order changes in (B 18) when k changes by $\mathrm{i}\epsilon$; so that, as (A 5) for K implies,

$$\bar{k} \text{ changes by } -\mathrm{i}\epsilon, \quad K \text{ by } \mathrm{i}\epsilon k K^{-1} \quad \text{and} \quad \bar{K} \text{ by } -\mathrm{i}\epsilon\bar{k}\bar{K}^{-1}. \tag{B 25}$$

These changes take place, however, from initial values with k real so that $k=\bar{k}$.

It will suffice to display the calculation for just the first term in (B 18), which can be written as

$$\tfrac{1}{4}\omega^{-1}V^2(K+\bar{K}) \quad \text{and changes by} \quad \tfrac{1}{4}\omega^{-1}V^2\,\mathrm{i}\epsilon(kK^{-1}-\bar{k}\bar{K}^{-1}). \tag{B 26}$$

With $k=\bar{k}$, this change becomes

$$\tfrac{1}{2}\omega^{-1}V^2\epsilon(\operatorname{Im}K)k\,|K|^{-2}. \tag{B 27}$$

The corresponding calculation for the second term is extremely lengthy, although completely straightforward. The change in the whole expression (B 18), including both terms, can be written

$$\tfrac{1}{2}\omega^{-1}V^2\epsilon\operatorname{Im}K\left[-\frac{|K-k|^2}{4(\operatorname{Re}K)^3}+\frac{k}{|K|^2}\left(\frac{\operatorname{Im}K}{\operatorname{Re}K}\right)^2+\frac{2k}{|K+k|^2}\right]. \tag{B 28}$$

Here, the negative first term dominates for small κ (that is, in the Stokes-layer limit). The other two terms – beginning with one similar in general appearance to (B 27) – are positive; and the last one becomes the leading term for large κ when K is close to k. However, this is a limit in which (B 28) is tending to zero.

With $V^2\epsilon$ replaced by $V\mathrm{d}V/\mathrm{d}x$ the additional shear-stress streaming (B 28) may be written as

$$-\tfrac{1}{4}V(\mathrm{d}V/\mathrm{d}x)\,\omega^{-1}\tau_1(\kappa) \tag{B 29}$$

in terms of a non-dimensional function $\tau_1(\kappa)$ of the non-dimensional wavenumber (A 6). Figure 13 shows how the variation of $\tau_1(\kappa)$ takes a very different form from that of $\sigma(\kappa)$; thus, $\tau_1(\kappa)$ changes much more steeply for small κ, and in the opposite direction, causing it to take negative values for $\kappa > 0.2$ before finally rising to its asymptote of zero for large κ.

We show in Appendix C that these characteristics of the additional shear-stress streaming mimic closely those of the rather larger normal-stress streaming. Just as in the Stokes-layer limit, then, the additional shear-stress streaming represents a moderate numerical enhancement of the normal-stress streaming.

Appendix C. High-wavenumber modifications to normal-stress streaming

C.1. *Introduction*

In this Appendix we make one final use of those locally two-dimensional flow fields that were derived in Appendix A for wavenumbers comparable to the reciprocal of the Stokes-boundary-layer thickness. We employ them to calculate the normal-stress streaming forced by such gradients of the Reynolds normal stress

$$\rho\langle u^2\rangle \tag{C 1}$$

in the x-direction as may accompany wave growth or decay.

In this calculation we are faced with a classical conundrum in a new form. Gradients of Reynolds stresses are known to produce no effective forcing of streaming motions in flow regions with no dissipation, such as regions external to boundary layers. On the other hand, the mean value (C 1) takes non-zero values outside a Stokes boundary layer; and we are faced, therefore, with the problem of how to express the fact that only the variations in (C 1) within the region of dissipation can produce forcing.

Three solutions to this problem suggest themselves, in ascending order of sophistication. All are equivalent in the Stokes-layer limit, but only the third continues to be available at higher wavenumbers.

The first of these solutions simply argues that, since no effective forcing is provided by the Reynolds stress (C 1) in the region external to the boundary layer, the associated streaming motions must be forced purely by the difference

$$\rho(\langle u^2\rangle - \langle u^2\rangle^{\mathrm{ext}}) \tag{C 2}$$

between the stress (C 1) and its value in the *exterior* flow just outside the boundary layer. This effective forcing (C 2) is exerted only within the very thin Stokes layer, and tends to zero at its edge. The associated Euler mean motion u_{E}, as defined in Appendix B, is governed by a balance

$$\rho\frac{\partial}{\partial x}(\langle u^2\rangle - \langle u^2\rangle^{\mathrm{ext}}) = \mu\frac{\partial^2 u_{\mathrm{E}}}{\partial y^2} \tag{C 3}$$

between the gradient of this stress difference (C 2) and the viscous force which, within that thin layer, resists the Euler mean motion.

A second solution – still using the boundary-layer approximation – goes 'back to fundamentals' and recalls why gradients of Reynolds stress produce no streaming in dissipation-free regions external to boundary layers. This is because motions in such regions are irrotational; accordingly, those combined gradients forcing the Euler mean velocity component u_{E} which, by the equation of continuity, can be written

$$\rho\frac{\partial}{\partial x}\langle u^2\rangle + \rho\frac{\partial}{\partial y}\langle uv\rangle = \rho\left\langle u\frac{\partial u}{\partial x} + v\frac{\partial u}{\partial y}\right\rangle, \tag{C 4}$$

may be rewritten as

$$\rho\left\langle u\frac{\partial u}{\partial x} + v\frac{\partial v}{\partial x}\right\rangle = \rho\frac{\partial}{\partial x}(\tfrac{1}{2}\langle u^2\rangle + \tfrac{1}{2}\langle v^2\rangle) \tag{C 5}$$

and balanced just by a static distribution of mean pressure

$$p_{\mathrm{E}} = -\tfrac{1}{2}\rho(\langle u^2\rangle + \langle v^2\rangle), \tag{C 6}$$

whose gradient in the y-direction is similarly found to balance the Reynolds stress gradients forcing the y-component v_E of Euler mean velocity.

Equation (C 3) may then be interpreted as stating that a gradient of the Reynolds normal stress (C 1) is opposed by a combination of (i) the viscous-force term on the right-hand side of (C 3) and (ii) a mean pressure gradient

$$-\partial p_E/\partial x \tag{C 7}$$

which, on the boundary-layer approximation, can be evaluated with p_E taken as its value in the flow just outside the boundary layer. In the present problem, for example, where in this exterior flow we have

$$\langle u^2\rangle = \langle v^2\rangle \quad \text{as well as} \quad \langle uv\rangle = 0, \tag{C 8}$$

the force (C 7) with p_E given by (C 6) accounts for the whole of the $\langle u^2\rangle^{\text{ext}}$ term in (C 3); whereas there is no corresponding term (since $\langle uv\rangle^{\text{ext}} = 0$) in the equation

$$\rho\frac{\partial}{\partial y}\langle uv\rangle = \mu\frac{\partial^2 u_E}{\partial y^2} \tag{C 9}$$

of which the integrated form (B 7) was used in Appendix B to calculate the shear-stress streaming component of the Euler mean motion.

A third solution, however, is still more valuable because it avoids making any boundary-layer approximation. It goes even further 'back to fundamentals'; that is, to Kelvin's theorem, which explains precisely why irrotational flows must remain irrotational whereas sources of new vorticity can exist only in regions with dissipation. This suggests that we try to characterize normal-stress streaming, not in terms of *momentum sources* for the Euler mean motion as in (C 3), but in terms of *vorticity sources* for the Euler mean vorticity

$$\omega_E = \partial u_E/\partial y - \partial v_E/\partial x. \tag{C 10}$$

If we do this we avoid any need to use boundary-layer approximations such as the constancy of pressure across a boundary layer. Pressure is eliminated between equations

$$\left.\begin{aligned}\rho\frac{\partial}{\partial x}\langle u^2\rangle + \rho\frac{\partial}{\partial y}\langle uv\rangle &= -\frac{\partial p_E}{\partial x} + \mu\nabla^2 u_E,\\ \rho\frac{\partial}{\partial x}\langle uv\rangle + \rho\frac{\partial}{\partial y}\langle v^2\rangle &= -\frac{\partial p_E}{\partial y} + \mu\nabla^2 v_E\end{aligned}\right\} \tag{C 11}$$

governing the Euler mean flow, so as to obtain an equation

$$\rho\frac{\partial^2}{\partial x\partial y}\langle u^2 - v^2\rangle + \rho\left(\frac{\partial^2}{\partial y^2} - \frac{\partial^2}{\partial x^2}\right)\langle uv\rangle = \mu\nabla^2\omega_E \tag{C 12}$$

for the mean vorticity (C 10).

Absolutely no boundary-layer approximation is needed, furthermore, for us to conclude that second derivatives $\partial^2/\partial x^2$ of mean values in (C 12) are negligible compared with their corresponding derivatives $\partial^2/\partial y^2$ with respect to y. Such mean values (for example, the integrand in (B 18), which represents $\langle uv\rangle$) vary with y at least as steeply as e^{-2ky} for all κ (and, for small κ when a Stokes layer exists, even more steeply) whereas logarithmic derivatives of mean values in the x-direction are

already taken as much smaller in magnitude than $2k$ when we apply high-frequency wave asymptotics.

Equation (C 12) can correctly be approximated, then, as

$$\rho\frac{\partial^2}{\partial x\partial y}\langle u^2-v^2\rangle+\rho\frac{\partial^2}{\partial y^2}\langle uv\rangle=\mu\frac{\partial^2}{\partial y^2}\omega_{\mathrm{E}}. \tag{C 13}$$

The solution of this linear equation of ω_{E} subject to the boundary condition (B 6) can be written as the sum of two solutions:

(i) a vortex-sheet solution with $\omega_{\mathrm{E}}=\nu^{-1}\langle uv\rangle$ in a thin layer separating the solid boundary, where condition (B 6) is satisfied, from an exterior motion where the Euler mean motion is given by (B 8) for the shear-stress streaming; and

(ii) a second vortex-sheet solution satisfying a zero boundary condition

$$u_{\mathrm{E}}=0 \quad \text{on} \quad y=0 \tag{C 14}$$

(since solution (i) already satisfies condition (B 6) in full) and with the vorticity ω_{E} satisfying

$$\rho\frac{\partial}{\partial x}\langle u^2-v^2\rangle=\mu\frac{\partial\omega_{\mathrm{E}}}{\partial y}. \tag{C 15}$$

In the rest of this Appendix we calculate the strength of this vortex sheet, which, because of the boundary condition (C 14), represents the normal-stress streaming at its edge.

Before doing so we note, however, that in the Stokes-layer limit (C 15) coincides with the equation (C 3) that was derived by either of the first two approaches. This is because v is necessarily constant across a Stokes boundary layer, so that $\langle v^2\rangle$ is equal to its exterior value, which (C 8) identifies with that of $\langle u^2\rangle$.

C.2. *Equations for normal-stress streaming*

The distribution ω_{E} of vorticity within the vortex sheet specified by (C 15) may be written

$$\omega_{\mathrm{E}}=-\nu^{-1}\frac{\partial}{\partial x}\int_y^\infty\langle u^2-v^2\rangle\,\mathrm{d}y, \tag{C 16}$$

where the upper limit represents, of course, the edge of the region within which the integrand is non-zero. The normal-stress streaming u_{S} is given as the vortex sheet's total strength (velocity change across it)

$$u_{\mathrm{S}}=\int_0^\infty\omega_{\mathrm{E}}\,\mathrm{d}y=-\nu^{-1}\frac{\partial}{\partial x}\int_0^\infty\langle u^2-v^2\rangle\,y\,\mathrm{d}y. \tag{C 17}$$

Now (A 4) allow us to express the mean value $\langle u^2-v^2\rangle$ as

$$\begin{aligned}\langle u^2-v^2\rangle&=\tfrac{1}{2}|A|^2(|\mathrm{e}^{-ky}-\mathrm{e}^{-Ky}|^2-|\mathrm{e}^{-ky}-kK^{-1}\mathrm{e}^{-Ky}|^2)\\&=\tfrac{1}{2}|A|^2\{(1-k^2|K|^{-2})\,\mathrm{e}^{-2y\,\mathrm{Re}\,K}-2\,\mathrm{e}^{-ky}\,\mathrm{Re}\,[(1-kK^{-1})\,\mathrm{e}^{-Ky}]\},\end{aligned} \tag{C 18}$$

so that the integral on the right-hand side of (C 17) is equal to

$$\tfrac{1}{2}|A|^2\{(1-k^2|K|^{-2})\,(2\,\mathrm{Re}\,K)^{-2}-2\,\mathrm{Re}\,[(1-kK^{-1})\,(k+K)^{-2}]\}. \tag{C 19}$$

Here, the real part of the expression in square brackets may be evaluated and then simplified as

$$k(3|K|^2-2k\,\mathrm{Re}\,K-k^2)\,|K|^{-2}\,|K+k|^{-2}\,(2\,\mathrm{Re}\,K)^{-1}. \tag{C 20}$$

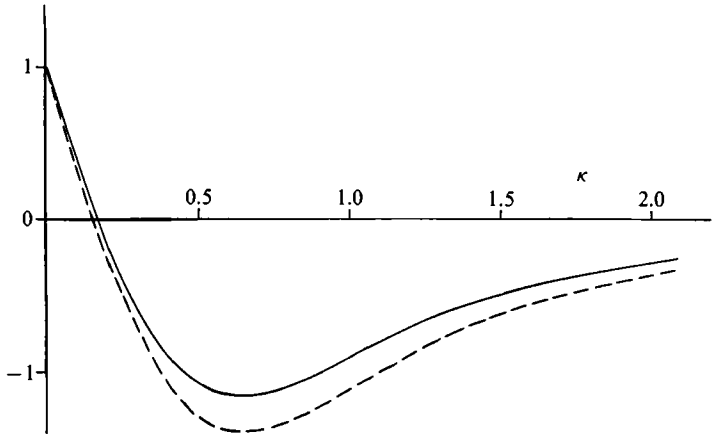

FIGURE 14. Here, the broken line gives the coefficient $\tau_2(\kappa)$ by which normal-stress streaming (C 23) is modified at high wavenumbers. The solid line plots $\tau(\kappa)$, defined in (C 25) as that linear combination of $\tau_1(\kappa)$ and $\tau_2(\kappa)$ which modifies – as (C 26) shows – the term due to wave growth or decay in the classical acoustic-streaming formula.

With this form used in (C 19), and with A substituted in terms of V from (A 5), the integral on the right-hand side of (C 17) can be rewritten as

$$V^2 \frac{|K|^2 - k^2 - 4k \operatorname{Re} K(3|K|^2 - 2k \operatorname{Re} K - k^2)|K+k|^{-2}}{8(\operatorname{Re} K)^2 |K-k|^2}, \tag{C 21}$$

and thence as

$$\frac{\nu V^2}{4\omega}\tau_2(\kappa) \quad \text{with} \quad \tau_2(\kappa) = \frac{\operatorname{Im} K}{|K-k|^2}\left\{\frac{|K|^2-k^2}{\operatorname{Re} K} - 4k\frac{3|K|^2 - 2k \operatorname{Re} K - k^2}{|K+k|^2}\right\}. \tag{C 22}$$

Therefore, the normal-stress streaming (C 17) takes the form

$$u_S = -\tfrac{1}{2}V(\mathrm{d}V/\mathrm{d}x)\,\omega^{-1}\tau_2(\kappa) \tag{C 23}$$

in terms of a non-dimensional function $\tau_2(\kappa)$ of the non-dimensional wavenumber (A 6).

C.3. *Physical discussion of normal-stress streaming*

Figure 14 shows that $\tau_2(\kappa)$ varies (broken line) in a way rather similar to that illustrated for $\tau_1(\kappa)$ in figure 13. In the Stokes-layer limit of small κ, (C 23) agrees with classical conclusions on normal-stress streaming because $\tau_2 = 1$. As κ increases, however, $\tau_2(\kappa)$ falls quite steeply and soon takes negative values (somewhat larger in magnitude than those taken by τ_1) before finally tending to its asymptote of zero from below.

These results deduced by calculation from the fundamental equation (C 15) can also be interpreted physically. Near the vibrating solid boundary, a normal stress $\rho\langle v^2\rangle$ in the y-direction is substantial but can readily be balanced, as the second of equations (C 11) shows, by an equal and opposite term in the mean pressure p_E, whose gradient in the x-direction is then available to oppose the gradient of the x-component $\rho\langle u^2\rangle$ of normal stress. Thus, it is only the difference $\rho\langle u^2 - v^2\rangle$ whose gradient forces normal-stress streaming.

Now, in the Stokes-layer limit, the distribution of $\langle u^2\rangle$ near the solid boundary is as shown (solid line) in figure 15. This reminds us how a Stokes layer differs from

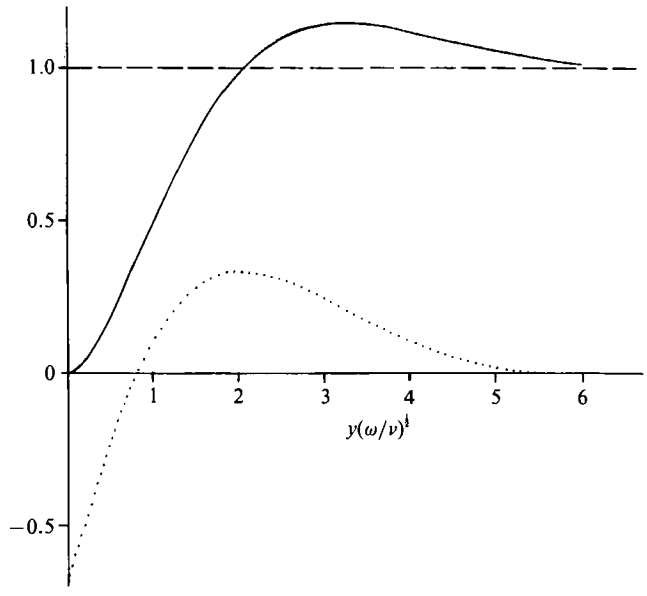

FIGURE 15. This shows the distributions of $\langle u^2 \rangle$ (solid line) and $\langle v^2 \rangle$ (broken line) in the Stokes-layer limit, both being made non-dimensional through division by $\frac{1}{2}V^2$. Note that these distributions give the integral $\int_0^\infty (\langle u^2 \rangle - \langle v^2 \rangle)\, y\, \mathrm{d}y$ a positive value. Also, the integral $\int_y^\infty (\langle u^2 \rangle - \langle v^2 \rangle)\, \mathrm{d}y$, made non-dimensional through division by $\frac{1}{2}V^2(\nu/\omega)^{\frac{1}{2}}$, is shown (dotted line – with, evidently, a positive integral from 0 to ∞).

steady-flow boundary layers in that velocities take values near the outer edge which exceed those in the exterior flow just outside the layer (figure 5). The explanation lies in the oscillatory character of vorticity production at the solid surface, and in the subsequent diffusion of that vorticity through the layer, which causes vorticities (and so also velocity gradients) in outer parts of the layer to be of opposite sign to those near the wall.

The broken line in figure 15, besides being the asymptote of the plain line, depicts also the uniform variations of $\langle v^2 \rangle$ in the Stokes-layer limit. It is the fact that $\langle u^2 \rangle$ exceeds $\langle v^2 \rangle$ in the outer parts of the layer (where y is greatest) that makes the integral in (C 17) take a positive value in that limit.

In further illustration of the same point, the dotted line in figure 15 gives the distribution of the integral in (C 16), determining that distribution of vortex-sheet vorticity whose integrated value is the streaming velocity (C 17). Clearly this dotted line has a positive integral across the sheet.

As κ increases, on the other hand, the distributions of u and v change markedly, in the general direction of those distributions for large κ that were plotted in figure 11, with amplitudes everywhere greater for v than for u. Then the integral in (C 17) rapidly becomes negative, although tending to zero for large wavenumber as the sheet gets thinner and thinner.

C.4. *General discussion of high-wavenumber streaming*

For waves with spatial growth or decay, the combined effect of the two streaming components (B 29) and (C 23) may be written

$$u_S = -\tfrac{3}{4}V(\mathrm{d}V/\mathrm{d}x)\,\omega^{-1}\tau(\kappa), \tag{C 24}$$

where the equation

$$3\tau(\kappa) = \tau_1(\kappa) + 2\tau_2(\kappa) \tag{C 25}$$

defines $\tau(\kappa)$ as the non-dimensional factor modifying, at high wavenumbers the classical Stokes-layer result. This result, often known (Lighthill 1978*a*) as Rayleigh's Law of Streaming, states that, for those *standing waves* which Rayleigh principally studied, the streaming velocity takes the form (C 24) with $\tau = 1$ in the Stokes-layer limit; although for *travelling waves*, of course, an additional term (B 9) appears.

The complete streaming motion for travelling waves, then, takes the form

$$u_S = \tfrac{1}{4}V^2 k\omega^{-1}\sigma(\kappa) - \tfrac{3}{4}V(\mathrm{d}V/\mathrm{d}x)\,\omega^{-1}\tau(\kappa) \qquad \text{(C 26)}$$

immediately outside the 'vortex sheet' distribution of mean vorticity (C 10). Here, as κ increases, $\sigma(\kappa)$ rises gradually from 1 to 2 as in figure 13; while figure 14 shows that the form (solid line) of the other modifying factor $\tau(\kappa)$ is intermediate (as (C 25) implies) between those of $\tau_1(\kappa)$ and $\tau_2(\kappa)$.

On the right-hand side of (C 26), the term which retains its importance for all wavenumbers is the first one, representing regular shear-stress streaming. In an extreme Stokes-layer limit of very small κ, this Euler mean motion just outside the Stokes layer (that is, at a point where $\mathrm{e}^{-\kappa y}$ is negligible and yet e^{-ky} is approximately 1) takes a value equal to one-quarter of the 'Stokes drift' expression $V^2 k\omega^{-1}$ for the irrotational motions near such a point. (The Lagrange mean motion is, of course, the sum of the two.)

For very large κ, by contrast, the regular shear-stress streaming rises from one-quarter to one-half of that 'Stokes drift' associated with a (then) purely hypothetical irrotational flow satisfying the boundary condition on v. This change from one-quarter to one-half intriguingly parallels a corresponding change (see Appendix A) in the 'excess' dissipation rate.

For the waves on the basilar membrane, of course, we are specially concerned with the region of spatial decay of wave amplitude ($\mathrm{d}V/\mathrm{d}x < 0$) from its peak value. Equation (C 26) shows that, in such a region, the regular shear-stress streaming just discussed is augmented by the effects of both additional shear-stress streaming and also normal-stress streaming provided κ remains small; on the other hand, it is somewhat diminished for larger values of κ.

REFERENCES

Allen, J. B. 1977 Two-dimensional cochlear fluid model: new results. *J. Acoust. Soc. Am.* **61**, 110–119.

Andrews, D. G. & McIntyre, M. E. 1978 An exact theory of nonlinear waves on a Lagrangian-mean flow. *J. Fluid Mech.* **89**, 609–646.

Ashmore, J. F. 1987 A fast motile response in guinea pig outer hair cells: the cellular basis of the cochlear amplifier. *J. Physiol.* **388**, 323–347.

Ashmore, J. F. 1989 Transducer motor coupling in cochlear outer hair cells. In *Cochlear Mechanisms – Structure, Function, and Models* (ed. J. P. Wilson & D. T. Kemp) pp. 107–116. Plenum.

Békésy, G. von 1960 *Experiments in Hearing*. McGraw-Hill.

Happel, J. & Brenner, H. 1965 *Low Reynolds Number Hydrodynamics*. Philadelphia: SIAM.

Johnstone, B. M., Taylor, K. J. & Boyle, A. J. 1970 Mechanics of the guinea pig cochlea. *J. Acoust. Soc. Am.* **47**, 504–509.

Kemp, D. T. 1978 Stimulated acoustic emissions from the human auditory system. *J. Acoust. Soc. Am.* **64**, 1386–1391.

Kemp, D. T. 1980 Towards a model for the origin of cochlear echoes. *Hearing Res.* **2**, 533–548.

Lighthill, J. 1978*a* Acoustic streaming. *J. Sound Vib.* **61**, 391–418.

Lighthill, J. 1978*b* *Waves in Fluids*. Cambridge University Press.

LIGHTHILL, J. 1981 Energy Flow in the cochlea. *J. Fluid Mech.* **106**, 149–213.

LIGHTHILL, J. 1983 Advantages from describing cochlear mechanics in terms of energy flow. In *Mechanics of Hearing* (ed. E. de Boer & M. A. Viergever), pp. 63–71. Delft University Press.

LIGHTHILL, J. 1991 Biomechanics of hearing sensitivity. *Trans. ASME: J. Vib. Acoust.* **113**, 1–13.

RAYLEIGH, LORD 1896 *Theory of Sound*, 2nd Edn. Macmillan (also, Dover reprint, 1945).

RHODE, W. S. 1971 Observations of the vibration of the basilar membrane in squirrel monkeys using the Mössbauer technique. *J. Acoust. Soc. Am.* **49**, 1218–1231.

SELLICK, P. M., PATUZZI, R. & JOHNSTONE, B. M. 1982 Measurement of basilar membrane motion in the guinea pig using the Mössbauer technique. *J. Acoust. Soc. Am.* **72**, 131–141.

STEELE, C. R. 1974 Behaviour of the basilar membrane with pure-tone excitation. *J. Acoust. Soc. Am.* **55**, 148–162.

STEELE, C. R. 1976 Cochlear mechanics. In *Handbook of Sensory Physiology*, vol. v/3: *Auditory System: Clinical and Special Topics* (ed. W. C. Keidel & W. D. Neff), pp. 443–478. Springer.

STEELE, C. R. & TABER, L. A. 1979 Comparison of 'WKB' and finite difference calculations for a two-dimensional cochlear model. *J. Acoust. Soc. Am.* **65**, 1001–1006.

VOLDŘICH, L. 1978 Mechanical properties of basilar membrane. *Acta Otolaryngol.* **86**, 331–335.

VOLDŘICH, L. 1983 Experimental and topographical morphology in cochlear mechanics. In *Mechanics of Hearing* (ed. E. de Boer & M. A. Viergever), pp. 163–167. Delft University Press.

WATSON, G. N. 1944 *Theory of Bessel Functions*, 2nd Edn. Cambridge University Press.

ZWEIG G. 1976 Basilar membrane motion. *Cold Spring Harbor Symp. Quantitative Biol.* **40**, 619–633.